HHS Public Access

Author manuscript

Magn Reson Med. Author manuscript; available in PMC 2024 March 05.

Published in final edited form as:

Magn Reson Med. 2023 May ; 89(5): 2024–2047. doi:10.1002/mrm.29572.

Current state and Guidance on Arterial Spin Labeling Perfusion MRI in Clinical Neuroimaging

Thomas Lindner, PhD,
Department of Diagnostic and Interventional Neuroradiology, University Hospital Hamburg-Eppendorf, Hamburg, Germany

Divya S. Bolar, MD PhD,
Center for Functional Magnetic Resonance Imaging, Department of Radiology, University of California San Diego, San Diego, CA, USA

Eric Achten, MD PhD,
Department of Radiology and Nuclear Medicine, Ghent University, Ghent, Belgium

Frederik Barkhof, MD PhD,
Department of Radiology and Nuclear Medicine, Amsterdam Neuroscience, Amsterdam University Medical Center, Amsterdam, The Netherlands; Queen Square Institute of Neurology and Centre for Medical Image Computing, University College London, UK

António J. Bastos-Leite, MD PhD,
University of Porto, Faculty of Medicine, Porto, Portugal

John A. Detre, MD,
Department of Neurology, University of Pennsylvania, Philadelphia PA USA

Xavier Golay, PhD,
UCL Queen Square Institute of Neurology, University College London, London, UK.

Matthias Günther, PhD,
(1) University Bremen, Germany; (2) Fraunhofer MEVIS, Bremen, Germany; (3) mediri GmbH, Heidelberg, Germany

Danny JJ Wang, PhD,
Stevens Neuroimaging and Informatics Institute, Keck School of Medicine, University of Southern California, Los Angeles CA USA

Sven Haller, MD, MSc,
(1) CIMC - Centre d'Imagerie Médicale de Cornavin, Place de Cornavin 18, 1201 Genève 1201 Genève (2) Department of Surgical Sciences, Radiology, Uppsala University, Uppsala, Sweden (3) Faculty of Medicine of the University of Geneva, Switzerland. Department of Radiology, Beijing Tiantan Hospital, Capital Medical University, Beijing, 100070, P. R. China

Silvia Ingala, MD,

[*]corresponding Author, Contact Info: Henk(-Jan) MM Mutsaerts, MD PhD, Dep. Radiology & Nuclear Medicine, Location Vumc PK −1X.112, de Boelelaan 1117, 1081 HV Amsterdam, h.j.mutsaerts@amsterdamumc.nl.

Department of Radiology and Nuclear Medicine, Amsterdam Neuroscience, Amsterdam University Medical Center, Amsterdam, The Netherlands

Hans R Jäger, MD PhD,
UCL Queen Square Institute of Neuroradiology, University College London, London, UK.

Geon-Ho Jahng, PhD,
Department of Radiology, Kyung Hee University Hospital at Gangdong, College of Medicine, Kyung Hee University, Seoul, Republic of Korea

Meher R. Juttukonda, PhD,
(1) Athinoula A. Martinos Center for Biomedical Imaging, Department of Radiology, Massachusetts General Hospital, Charlestown MA USA (2) Department of Radiology, Harvard Medical School, Boston MA USA

Vera C. Keil, MD,
Department of Radiology and Nuclear Medicine, Cancer Center Amsterdam, Amsterdam University Medical Center, Amsterdam, The Netherlands

Hirohiko Kimura, MD PhD,
Department of Radiology, Faculty of Medical sciences, University of Fukui, Fukui, JAPAN

Mai-Lan Ho, MD [Associate Professor of Radiology],
Nationwide Children's Hospital and The Ohio State University, Columbus, OH, USA

Maarten Lequin, MD PhD,
Division Imaging & Oncology, Department of Radiology & Nuclear Medicine | University Medical Center Utrecht & Princess Máxima Center for Pediatric Oncology, Utrecht, The Netherlands

Xin Lou, MD,
Department of Radiology, Chinese PLA General Hospital, Beijing, China

Jan Petr, PhD,
(1) Helmholtz-Zentrum Dresden-Rossendorf, Institute of Radiopharmaceutical Cancer Research, Dresden, Germany (2) Department of Radiology and Nuclear Medicine, Amsterdam Neuroscience, Amsterdam University Medical Center, Amsterdam, The Netherlands

Nandor Pinter, MD,
Dent Neurologic Institute, Buffalo, NY, USA. University at Buffalo Neurosurgery, Buffalo, NY, USA.

Francesca B. Pizzini, MD PhD,
Radiology Institute, Dept. of Diagnostic and Public Health, University of Verona, Verona, Italy

Marion Smits, MD PhD,
(1) Department of Radiology & Nuclear Medicine, Erasmus MC, Rotterdam, The Netherlands (2) The Brain Tumour Centre, Erasmus MC Cancer Institute, Rotterdam, The Netherlands

Magdalena Sokolska, PhD,
Department of Medical Physics and Biomedical Engineering University College London Hospitals NHS Foundation Trust, UK

Greg Zaharchuk, MD PhD,
Stanford University, Stanford, CA, USA

Henk JMM Mutsaerts, MD PhD*
Department of Radiology and Nuclear Medicine, Amsterdam Neuroscience, Amsterdam University Medical Center, Amsterdam, The Netherlands

Abstract

This article focuses on clinical applications of arterial spin labeling (ASL) and is part of a wider effort from the International Society for Magnetic Resonance in Medicine (ISMRM) Perfusion Study Group to update and expand on the recommendations provided in the 2015 ASL consensus paper. While the 2015 consensus paper provided general guidelines for clinical applications of ASL MRI, there was a lack of guidance on disease-specific parameters. Since that time, the clinical availability and clinical demand for ASL MRI has increased. This position paper provides guidance on using ASL in specific clinical scenarios, including acute ischemic stroke and steno-occlusive disease, arteriovenous malformations and fistulas, brain tumors, neurodegenerative disease, seizures/epilepsy, and pediatric neuroradiology applications, focusing on disease-specific considerations for sequence optimization and interpretation. We present several neuroradiological applications in which ASL provides unique information essential for making the diagnosis. This guidance is intended for anyone interested in using ASL in a routine clinical setting — i.e., on a single-subject basis rather than in cohort studies — building on the previous ASL consensus review.

Introduction

Arterial Spin Labeling (ASL) is a non-invasive magnetic resonance imaging (MRI) technique capable of quantifying and visualizing regional cerebral blood flow (CBF) in vivo. ASL has been available on clinical MRI scanners for well over a decade and a growing body of literature supports the utility of ASL not only as an alternative to contrast-based perfusion MRI, but also for selected pathologies in which ASL has particular sensitivity and may add specific clinical information (1). While several clinical applications of ASL have been suggested (2–4), the routine clinical use of ASL in non-specialized clinical centers remains limited. Recent ASL developments have been focused mainly on technical advances in the ASL sequence itself that are not ready yet for clinical use and may make ASL seem unnecessarily complex to the clinician. This includes improvements in the number of acquired time points (5,6), optimized post-processing (7–10), and more accurate CBF quantification (11)(12). This paper aims to reduce the apparent complexity of ASL by providing guidance for the everyday use of ASL.

In 2015, the ISMRM perfusion study group and the European COST-AID action BM1103 (https://www.cost.eu/actions/BM1103/) published a consensus statement for acquisition parameters, processing strategies, and basic image interpretation (13). This consensus statement led to a rise in clinical applications of ASL and the harmonization of ASL product sequences across MRI vendors. Based on consensus recommendations, many MRI scanners now offer a single post-labeling delay (PLD) background-suppressed 3D pseudo-continuous ASL (PCASL) sequence. This implementation provides -compared to other commonly used ASL sequences such as PASL- a higher signal-to-noise ratio (SNR) in clinically feasible imaging times, is robust under a variety of conditions and for various pathologies, and

allows quantitative CBF measurement. This so-called ‘white paper ASL sequence’ can be easily added to brain MRI protocols, even in non-specialized centers. The 2015 consensus statements recommended the same sequence parameters for 1.5T and 3T scanners, which is also true in this guidance paper.

Despite its technological readiness, more effort is needed to incite wider clinical adoption of ASL. One conclusion reached at the 2019 ISMRM ASL workshop at the University of Michigan, Ann Arbor (MI, USA) was that knowledge and education were lacking for clinical applications of ASL. Additionally, while the consensus recommendations on acquisition are still generally valid, additional guidelines can be helpful for specific clinical indications. Therefore, this position statement aims to provide guidance on the use of ASL across several disease areas for which ASL has shown utility. We aim to take the uncertainty out of using ASL in specific pathologies, and thereby encourage clinicians to use ASL in their daily clinical practice.

First, we provide protocol guidance for specific clinical indications as an extension to the 2015 protocol recommendations (13). Second, we provide guidance on crucial post-processing steps needed for clinical indications. Finally, we provide thoughts on the clinical interpretation and reporting of ASL CBF images. The guidance presented here is focused on the main disease areas in which ASL has shown to be a valuable tool for diagnosis, evaluating response to therapy, and monitoring disease progression. This paper is expected to be most useful for readers who already have a basic understanding of key ASL concepts and clinical applications.

Considerations for ASL use in a general neuroradiology setting

Highlights

- Clinical/Physiological
  - A 5-minute single-PLD sequence provides an overview of cerebral hemodynamics
  - Visual inspection of the mean subtraction image (relative perfusion map) is often sufficient
- Sequence
  - Double-check the position of the labeling plane
  - No need for advanced post-processing
  - Beware of apparent motion and the prior use of Gadolinium

Indications

In routine clinical practice, ASL perfusion MRI can provide useful hemodynamic information which would be otherwise unavailable, unless an external contrast agent is applied. Since the evaluation of regional perfusion is useful in many diseases, particularly when no prior imaging is available, ASL can be applied with the only restrictions being general MRI exclusion factors in all neurological diseases in which information about

blood supply is of interest. Furthermore, in clinical questions with unknown origin (e.g. “headache” or “unspecified neurological deficits”), ASL can be an additional help to state a diagnosis. In general, the authors suggest using the subsequently described simple sequence and using the information gained for the initial diagnosis (e.g. asymmetric perfusion) and using this information for further diagnostic tests that follow the initial assessment rather than trying to mitigate these artifacts by using advanced methods.

Acquisition

A general ASL sequence for use in patients without a clear indication should be easily applicable in a wide range of diseases and not include advanced post-processing methods, to provide a quick overview of the vascular situation. Thus, it is advised to follow the age-optimized consensus protocol (13) which uses single-delay, background-suppressed, vascular-suppression-disabled PCASL with a 3D readout, with a 2D EPI readout as a second option (Supplement Table 1). This sequence can also be seen as the go-to option when no modifications are possible and the department can only use this one set of parameters. Vascular suppression should be disabled to allow visualization of macrovascular signals in arteries (so-called arterial transit artifact (ATA)) and veins, which can provide valuable clinical information – sometimes critical to diagnosis. ATA occurs when labeled blood remains within the supplying arteries/arterioles, having not yet reached and distributed into the microvasculature and tissue. The labeled blood that should have been distributed to multiple distal voxels thus remains concentrated in a single proximal vessel voxel, resulting in a markedly hyperintense ASL signal. ATA can be found with too short PLD and distal to arterial stenoses or occlusions (that impede flow) or within circuitous collateral pathways.

When shorter protocols are necessary, the acquisition time can be reduced by decreasing the number of repetitions and/or increasing voxel size to maintain SNR. Of note, 3D ASL scans can include substantial blurring related to the acquisition or reconstruction (14,15), so that the final spatial resolution of 3D ASL may be lower than expected. In general, a 5 minutes ASL scan is sufficient for clinical interpretation, although longer imaging times may be helpful in certain cases, e.g., to more accurately characterize CBF in regions of susceptibility artifacts, or relatively low SNR or baseline perfusion ((16). However, the user should be aware that longer acquisition times increase the risk of motion artifacts.

Furthermore, the position of the PCASL labeling plane relative to the imaging slab can dramatically affect the ASL perfusion measurement. Ideally, the image volume and the labeling plane can be independently moved and rotated without restriction. In this case, the labeling plane is best-placed perpendicular to the spine at the level of the 2nd or 3rd cervical vertebra (17) - or about 4 cm below the base of the cerebellum. In this configuration, both the internal carotid and vertebral arteries should be nearly perpendicular to the labeling plane, resulting in symmetrically high labeling efficiency for both the anterior and posterior circulation (Figures 1 and 2). If a vessel scout is available, the labeling plane can be directly positioned roughly perpendicular to the internal carotid and vertebral arteries. Some commercially available PCASL sequences, however, do not allow free control of both the imaging volume and PCASL labeling plane as the vendor fixes (or hides the display of) the labeling plane in parallel to the imaging volume. Therefore, it is the neuroradiologists’ or

techs' task to choose whether the focus lies on optimizing labeling efficiency or acquiring the standard brain orientation. The authors suggest focussing on high labeling efficiency over standard orientation to avoid false-positive hypoperfusion as an artifact.

Post-processing

In most cases, the only required post-processing steps are (pairwise) control-label subtraction and averaging of the resultant subtraction series to provide perfusion-weighted maps. If possible, quantitative CBF maps should also be calculated and presented in both grayscale and color. Other, more advanced post-processing steps like outlier scrubbing and motion correction would likely take too much time in clinical routine and might detract clinicians.

Interpretation

Visual inspection of the average control-label subtraction — perfusion-weighted image — is often sufficient. Emphasis should be placed on identifying regions of hypoperfusion, hyperperfusion, ATA, and high-intensity venous signal. In addition, visually checking the unsubtracted control-label images and the M0 image can help to identify artifacts that induce spurious CBF signals. Importantly, ASL is often of great value when used as an adjunct to provide physiological information that complements structural imaging, thereby narrowing the differential and often even confirming the diagnosis. It should be noted that considerable physiological variability exists in cerebral perfusion (18) as perfusion values are dependent on age, sex, hematocrit, and exogenous factors such as caffeine, nicotine (19,20), or sedation (the latter being most important in pediatric imaging). There is currently no consensus on the level of restriction of these exogenous perfusion modifiers — e.g. restriction of caffeine or food intake before the exam — before performing ASL, but should be taken into account when the results are unclear. Another important factor is that gadolinium-based contrast agents should only be administered after ASL has been acquired, otherwise the ASL acquisition will be of too low and non-diagnostic quality due to the shortened blood T1 (2). In cases of multi-PLD acquisitions, the individual review of all PLD images can be cumbersome, and only the relevant series should be inspected in detail. Finally, as ASL is a subtraction technique, motion is particularly prone to producing erroneous images. In cases of head motion (control-label misalignment), the voxel-by-voxel subtraction does not work sufficiently and images can be corrupted. The advantage of ASL, however, is that re-scanning the ASL sequence is possible with only a minor time penalty.

Advanced considerations

Advanced techniques can be considered in more complex situations and when the initial assessment is done. This section only gives a brief overview of the methods, which are discussed pathology-specific in the subsequent sections. Such methods include multi-PLD acquisitions that can provide additional information on arterial transit times (ATT) and thus increase the diagnostic confidence of the images. This can be particularly helpful in areas of low perfusion (21) and arterial transit delays as well as for adding additional hemodynamic information by explicitly measuring ATT (22,23). Furthermore, the ATT artifacts can be corrected in multi-PLD acquisitions since the variation in PLDs allows for differentiating between early macrovascular signal or true hyperperfusion. However, because

of its complexity and challenges, multi-PLD approaches are currently not being seen as appropriate default protocols and only be performed in specific diseases as discussed later. Challenges include longer scan times (e.g. multiple single PLDs or complex Hadamard encoding) and post-processing of the individual time-points and potential dependence on the delay times (24). A valid alternative to multi-PLD can be using two single-PLD scans — one with regular PLD of 2000ms and an additional with longer PLD, e.g. 2500ms — to visualize two phases, mainly to distinguish between ATA and hyperperfusion. Individual adaptations are possible, depending on the experience of the user and expected ATT. Unlike contrast-agent based methods, ASL can provide absolute CBF quantification with an accuracy and reproducibility comparable to ^{15}O-H_2O PET (25), but may be influenced by various confounders such as long ATT (22,23), labeling efficiency (26), blood T1 or hematocrit (27), (27). While quantification of ASL images is possible, relative perfusion values can be sufficient and robust for many applications. As ASL is particularly sensitive to hemodynamic changes accompanying vascular disease and also to a lesser extent in normal aging, blood flow from the neck to the imaged region can be delayed and manifest as ATA (Figure 3). This can be visually categorized using the ATA score (28,29).

Acute ischemic stroke and steno-occlusive diseases

Highlights

- Clinical/Physiological
  - ASL has potential for visualizing collateral flow, identifying distal stenoses/occlusions and classifying mismatch
  - Arterial transit times are often prolonged in AIS/SOD, potentially leading to ATA and hypoperfusion overestimation
  - Cerebrovascular reserve (CVR) imaging is emerging as a useful application of ASL in SOD
- Sequence
  - Single-PLD consensus ASL is often sufficient for rapid evaluation of AIS/SOD hemodynamics, while multi-PLD potentially increases CBF accuracy and provides regional ATT information.
  - ASL-DWI mismatch is similar to PWI-DWI mismatch provided by DSC (with caveats).
  - ATA can identify collateral flow and distal stenoses/occlusions.
  - A long labeling duration, long PLD scan can be considered to mitigate transit delay effects (particularly if multi-PLD is unavailable).

Indication

Acute ischemic stroke (AIS) and steno-occlusive disease (SOD) involve stenosis or occlusion of the arteries that supply blood to the brain. A class of acute/subacute SOD includes vasculitis and reversible cerebral vasoconstriction syndrome (RCVS). Chronic SOD

refers to progressive narrowing of the intracranial and/or cervical arteries over time, which can eventually result in reduced CBF and AIS. As a compensatory response, patients often develop collateral pathways in an attempt to maintain CBF. Moyamoya, intracranial arterial stenosis, and extracranial carotid stenosis are prototypical chronic steno-occlusive processes that can be characterized by ASL.

Acquisition

Single-PLD PCASL without vascular suppression and using consensus recommendations is a reasonable option for AIS given its urgent nature and need for rapid clinical decision-making. It is important that vascular suppression is disabled to allow the visualization of ATA. Multi-PLD or single-PLD PCASL with long labeling duration and long PLD (e.g, 3000 ms/3000 ms) (31) attempts to mitigate transit delay effects and may be considered if multi-PLD is not available. Performing two single-PLD PCASL scans with different delay times (e.g. 1500 ms and 2500 ms) may also more accurately measure CBF and visualize collateral flow (32,33). When longitudinally assessing SOD, the optimal ASL parameter choice may simply be those used in the prior study (or studies) to allow for a properly matched comparison.

Post-processing

Standard ASL subtraction and perfusion map generation can be applied for single-PLD PCASL (13). Rigid interpretation of quantitative CBF maps is discouraged, as they will likely have regional inaccuracies due to transit delay effects. Multi-PLD data theoretically accounts for these effects and can be analyzed with the standard kinetic model for ASL (34)(35)

Interpretation: AIS

The transit time of the ASL label from the proximal arteries to the tissue (the ATT) is typically prolonged in both AIS with large vessel occlusion (LVO) and SOD. Single-PLD PCASL using consensus-recommended parameters thus will result in the label remaining within the macrovasculature at the time of imaging. This manifests as a hyperintense macrovascular ASL signal (ATA) and apparent perfusion deficits that correspond to regions of delayed transit.

Single-PLD PCASL subsequently provides important information in AIS. First, it has the potential for mismatch classification, as the reduced perfusion signal downstream to the LVO can be used to estimate ASL-DWI mismatch (36)(37)(38). Since PWI-DWI mismatch is used to identify adult patients who may benefit from mechanical thrombectomy (39)(40), ASL-DWI mismatch could play a similar role. However, since standard delay PCASL can potentially overestimate mismatch (36)(37)(38), cautious interpretation is required. Long delay, long PLD methods may improve accuracy, as will multi-PLD methods as they become more feasible in acute settings. ASL also allows collateral visualization, since ATA can be used to identify leptomeningeal collaterals, which are associated with better neurological outcomes in AIS with LVO (41)(42) (Figure 4). Finally, since ATA is highly sensitive to arterial occlusion, ASL can be used to detect occlusions in distal arterial branches and at bifurcations, which are occasionally missed by CTA and/or MRA (43–45).

Single-PLD PCASL can also be used to evaluate increased (luxury) perfusion within the infarct core after revascularization. This is associated with infarct stability (i.e. lack of expansion) (46), though has also been linked to an increased risk of hemorrhagic transformation (47) and reperfusion syndrome (48). Hyperperfusion in the absence of an infarct argues against ischemia and raises the possibility of stroke mimics such as seizure, encephalitis, or complex migraine, as well as reperfusion in the setting of transient ischemic attack (TIA). A physiologically normal appearing ASL study has a high negative predictive value for the presence of hemodynamically significant stenosis or occlusion (49).

As mentioned, accurate absolute CBF quantification in regions downstream to arterial occlusion is typically not possible with standard single-PLD PCASL due to long ATTs. Multi-PLD ASL, however, is often substantially more accurate in this setting, with highly significant correlations found between ASL-CBF and DSC-CBF and significant correlations found between ASL-ATT and DSC-Tmax; as such, multi PLD ASL may provide more accurate mismatch information (35). Single-PLD PCASL with long label and long delay will also reduce ATT sensitivity (Figure 5). However, both approaches will be limited in settings of extremely long ATT, which are sometimes present in AIS with LVO. In this regard, ATT-insensitive velocity-selective ASL (VSASL) holds promise to more accurately measure CBF in these settings (50,51).

Interpretation: Steno-occlusive disease

Single-PLD PCASL can also be used to identify stenoses and assess collateral robustness in SOD. In patients with carotid stenosis, the presence of ATA was found to be predictive of recent symptoms (52). Since most SOD cases are not urgent, more tailored approaches are possible. Patients with SOD may benefit from multi-PLD PCASL for more accurate evaluation of CBF and ATT in the presence of transit delays.

A separate CBF-related parameter called cerebrovascular reserve (CVR) reflects the brain's capacity to respond to increased demand and provides a useful biomarker for stroke risk stratification in chronic SOD. CVR testing involves comparing CBF measured at baseline and after administration of vasoactive agents that increase CBF (such as acetazolamide or inhaled CO2) to investigate regions with reduced CBF response are at higher risk for future ischemia. ASL holds great potential for this application, and while not yet widely used in the clinic, there are promising reports in the literature that use ASL-CVR to evaluate disease progression and the need for revascularization in chronic SOD ((53).

AVF/AVM

Highlights

- Clinical/Physiological
  - ASL allows for both initial diagnosis and monitoring after treatment
  - AV shunt lesions present in hyperintense signal in the nidus and/or draining veins
- Sequence

- For initial evaluation, single-PLD ASL is sufficient, for shunt flow characterization multi-PLD imaging provides deeper insights
- Relative CBF allows for detection and diagnosis while steal phenomenon evaluation is preferably performed using quantitative CBF data

Indication

ASL is well-suited to identify cerebral arteriovenous (AV) malformations (AVMs) and fistulas (AVFs) due to its exquisite sensitivity to AV shunting. Several studies have shown ASL to be both highly sensitive and specific for detecting AV shunt lesions (43,54,55), with up to 95% sensitivity and 90% specificity (54). ASL can detect small AVMs that would otherwise be missed by conventional MRI, e.g. in the setting of a ruptured AVM, in which susceptibility from blood products may mask the lesion on conventional imaging (43). This sensitivity arises from the high concentration of ASL label flowing through shunts as the label bypasses the microvascular/tissue network and is directly delivered to the venous circulation in AVFs and draining veins in AVMs.

Acquisition

Standard single-PLD PCASL using consensus recommended parameters is often sufficient for detecting AV shunt lesions by identifying nidal/venous ASL signal. Vascular suppression must be disabled to allow visualization of high flowing nidal/venous ASL signal. Multi-PLD PCASL can also be useful in facilitating detection by providing a dynamic, low-resolution angiographic assessment of the ASL label as it enters the shunt and then flows into the venous system. When multi-PLD ASL is not available, at least two ASL acquisitions with varying PLD could be utilized (e.g. 2000ms and 2500ms). Of note, spatial resolution is important for this application, thus multi-PLD ASL is not encouraged by the authors if it requires a reduction in spatial resolution or if the patient is unstable and likely to move during the acquisition.

Post-Processing

AVM/AVF detection and interpretation typically relies on standard ASL subtraction for qualitative perfusion values and thus, these images are therefore seen as the primary source of information. For an advanced diagnosis, especially when long-term follow-up imaging is planned, quantitative ASL can be used when evaluating shunt flow and tissue surrounding the AVF/AVM.

Interpretation

Evaluation of AV shunt lesions with ASL relies on identifying high macrovascular signal outside the arterial tree and within the nidus (for AVMs) and venous system (Figure 6). Hyperintense ASL signals within these vascular compartments can be seen even in slow-flow shunts. This is consistently observed with AV shunt lesions and forms the basis of evaluation by ASL in de novo shunts in those undergoing treatment. Complimentary MRI features on conventional MRI sequences should be taken into consideration, such as loss or attenuation of associated venous flow voids on T2-weighted images and the presence of

flow-related enhancement within veins on MR angiography. When there is ambiguity with regard to whether a high macrovascular ASL signal resides in an artery (i.e. ATA) or vein, multi-PLD can allow visualization of the label as it flows along the expected course of a vein to remove this ambiguity.

Studies have shown that ASL maintains its high sensitivity and specificity for AV shunting even after treatment, detecting residual shunt flow following stereotactic radiosurgery (56) and gamma-knife therapy (57,58), as well as shunt reduction after embolization (59,60). Similar principles employed for detection can also be applied for characterizing treatment response, specifically evaluating for nidal/venous signal that decreases post-therapy.

When quantifying ASL images, signal intensity within the nidus and draining vein have been shown to correlate well with the degree of early draining vein signal enhancement (a surrogate for the degree of AV shunting) (57). Perfusion in tissue adjacent to AVMs might be decreased, presumably due to steal phenomena (55,61). Because of its high sensitivity to arteriovenous shunting, ASL can be used to differentiate shunt-type lesions from developmental venous anomalies (DVA), most of which have normal ASL signal (62). DVAs are likely to present as incidental findings without associated clinical symptoms, and most are not of clinical significance.

A potential pitfall is jugular venous reflux, as labeled venous blood in the neck can travel superiorly into the venous sinuses. This could erroneously be interpreted as a venous ASL signal that has transited via shunting. In these cases, an additional MRA of the head should be performed to visualize the flow-related enhancement. If the enhancement is more intense inferior, this indicates the presence of a labeled venous signal coming from below. Alternatively, with multi-PLD ASL, the direction of ASL label flow can be distinguished.

Hyperintense ASL signal in venous sinuses may also be caused by labeled blood traversing the capillary bed without fully exchanging with tissue, e.g. in young adults with sickle cell anemia (SCA) in whom arterial velocities are elevated (63,64) and in some high-grade tumors with shunting. Therefore, care should be taken when interpreting venous ASL signals in the presence of clinical conditions where altered microvascular flow patterns are expected. In these cases, venous ASL signal could be indicative of capillary shunting (as opposed to physical arteriovenous shunt) and consequently reduced oxygen extraction efficiency (65).

Brain tumors

Highlights

- Clinical/Physiological
  - ASL can aid with brain tumor diagnosis and differentiating disease progression from pseudoprogression/radiation necrosis
  - Both the tumor and the peritumoral region need to be assessed
- Sequence

- Single-PLD ASL is sufficient, advanced methods are not necessary
- Quantification of data is not required
- Colormaps hold the potential to aid in interpretation

Indication

ASL can be used for most intra- and extra-axial brain tumors, whether primary (e.g. glioma) or secondary (e.g. metastasis), for initial diagnosis or monitoring. There is a correlation between ASL-calculated CBF with tumor histology, grade, and microvascular density (66,67). Commonly reported and recommended indications of ASL are the differentiation between tumor and non-tumoral pathologies (68) or between various types of brain tumors (69–71), grading and malignant transformation of primary brain tumors (72), and the differentiation between tumor progression and treatment-related radiological abnormalities (73)(74)(73). ASL has the advantage of being easier to model, rendering quantitative CBF measurements more directly accessible without the need for an arterial input function and without taking into account effects from blood-brain barrier (BBB) leakage as it would be the case for perfusion MRI using a gadolinium-based contrast agent (75).

Acquisition

The published recommendations from the ASL consensus paper (13) are valid for this application and thus can be readily used for clinical routine practice. There is currently no consensus on the need for multi-PLD methods in clinical routine imaging for brain tumors, though there may be some benefit for the accuracy of glioma grading (76). Since 3D spin-echo (spiral) ASL readout is much less sensitive to susceptibility artifacts than gradient-echo 2D EPI imaging, ASL is particularly helpful in the post-operative setting where susceptibility artifacts due to air and hemorrhage may occur (74).

Post-processing

Post-processing of ASL tumor data can be limited to a simple control-label subtraction to visualize the lesion. Several studies have shown that ASL and DSC imaging have a good interobserver correlation and reproducibility (72). Although conflicting results exist, these are attributed to differences in post-processing (72). Normalizing ASL difference images to normal-appearing (contralateral) tissue (gray or white matter, mirrored ROI, or cerebellum) may improve accuracy in tumor grading (72).

Interpretation

Interpretation of the final ASL images should be performed primarily on the mean perfusion images (Figure 7). Color-encoding these images may aid in highlighting subtle areas of abnormal perfusion. Combining the color-encoded and anatomical images either as an overlay or using a cross-referencing function is helpful for localization, but it should be kept in mind that the spatial resolution of ASL is lower than that of the anatomical images. Additionally, the use of colormaps is controversial in scientific and clinical presentation and thus needs to be carefully considered, and the visual impression might be exaggerated, therefore the use of color-encoding should only be performed alongside gray-scale images (77)(78). Lesions below 5–10 mm may be too small to characterize with ASL, which can

potentially result in a false negative for elevated tumor blood flow. This lower lesion size limit depends on the spatial resolution of the acquisition. Both the tumor and peritumoral region should be assessed for ASL hyperperfusion, elevated peritumoral blood flow can help differentiate high-grade gliomas from brain metastasis (69,70), since high-grade gliomas may demonstrate elevated both intratumoral and peritumoral perfusion, whereas hypervascular metastases will typically only show elevated perfusion within the tumor (69). It should be noted that because of the high background CBF of the brain, many metastases will appear isointense to hypoperfused relative to the cortex; the main exceptions to this are hypervascular metastases, such as renal cell carcinoma, thyroid carcinoma, melanoma, choriocarcinoma, and esthesioneuroblastoma, and some breast and lung cancer metastases. When analyzing longitudinal normalized data, interpretation should be done with caution since CBF changes were demonstrated in normal-appearing tissue after radio-chemotherapy (79,80). When evaluating progression vs. pseudoprogression, both manifest as increased lesion size and/or contrast enhancement in structural MRI, but in pseudoprogression, this is secondary to treatment rather than worsening disease. Differentiating between the two has important clinical implications, but can be difficult with conventional imaging alone. Perfusion imaging can be effective in making the distinction, with hyperperfusion suggestive of true progression and iso- to hypoperfusion more indicative of pseudoprogression. While both ASL and DSC perfusion imaging can be used, DSC can fail in regions of susceptibility, for example, due to blood products after tumor resection and near air-tissue interfaces of the skull base (Figure 8).

Adding ASL to the follow-up imaging protocol is useful as serial changes in relative tumor blood flow provide more information than a single time point assessment. However, ASL still has value when performed in the absence of baseline since a comparison with perfusion in the tissue of origin can then be made, though normalizing to the normal-appearing white matter is not always reliable after treatment, when perfusion in the white matter may be decreased. As a visual aid, the contralateral signal can be used as a reference; i.e. signal higher than that of the contralateral parenchyma can be considered as increased. Macrovascular artifacts are commonly seen in tumors with apparent CBF values exceeding 500 mL/min/100g in highly vascular tumors. While this can yield useful information about tumor vascularity, it is important to note that this signal does not represent true perfusion.

Neurodegenerative disease

Highlights

- Clinical/Physiological
  - ASL can be used for early detection of perfusion patterns suggestive of specific neurodegenerative disorders, in particular before volume loss or structural changes are apparent
  - Transit-times can be prolonged (physiological and pathological)
- Sequence

- Single-PLD consensus ASL is the method of choice, multi-PLD or other modifications are not seen as necessary. The sequence should be adapted to the age-recommended PLD value
- Quantification of data is not required
- Colormaps hold the potential to aid in interpretation

Indication

MRI has been traditionally used to exclude secondary causes of dementia, rather than diagnose a primary neurodegenerative disorder. While structural changes can be seen on MRI with primary disease, these typically become clinically apparent much later in disease progression, often after the diagnosis has been made clinically. ASL has the potential to detect perfusion changes in Alzheimer's Disease (AD) and other neurodegenerative conditions (81–83) before macroscopic volume loss or other structural changes are evident. Since the standard indications for e.g. memory loss in MRI exams are typically done without contrast agent, ASL is an ideal option for measuring perfusion in these patients. ASL has been proven to capture patterns of hypoperfusion in AD cohorts that are similar to the patterns obtained using Positron Emission Tomography (PET) and Single Photon Emission Computed Tomography (SPECT) (82,84–86). AD-related hypoperfusion has been demonstrated in the temporal, parietal, and posterior cingulate cortices (82)(86–88), the insula, and the hippocampus (89). Additionally, it has been shown to predict conversion from mild cognitive impairment (MCI) to AD (90). ASL also captures patterns of regional perfusion abnormalities in frontotemporal dementia (FTD) (91), dementia with Lewy bodies (DLB) (92,93), and Parkinson's disease (PD) (94), and may help differentiate between AD and FTD (88,95–97). In addition, ASL is a useful method to evaluate disease progression (98–100)(101). While ASL is not seen as a stand-alone diagnostic tool for neurodegenerative disease, it could act as an adjunct marker or screening tool to refer patients to FDG PET or amyloid or tau PET (in specialized centers) (102).

Acquisition

The age-related recommendations from the ASL consensus paper (13) are valid for neurodegenerative diseases. The PLD recommendation of 2000 ms may be sufficient in midlife patients for example with expected frontotemporal dementia (FTD), but should be increased in patients with expected poorer cerebrovascular health due to prolongation of the ATT (e.g. to 2500ms) (103,104).

Susceptibility-dependent geometric distortion and signal loss artifacts in the orbitofrontal and inferior-temporal cortices near the nasal and mastoid air spaces can be reduced in 2D EPI and 3D GRASE ASL readouts using reduced effective echo spacing with in-plane acceleration. The 3D FSE-spiral ASL does not suffer from signal loss or geometric distortion but can have blurring in these regions of high susceptibility, although this is reduced when using multiple segments (like 8 arms in GE's implementation) (105)(106).

Post-processing

Since neurodegenerative perfusion changes can be subtle, especially in the early phases, general physiological perfusion confounders have a relatively large effect on the interpretation of ASL perfusion images in the context of neurodegenerative disease. Partial volume correction (PVC) can be used to remove pseudo-hypoperfusion effects secondary to cerebral atrophy (107) for quantification of ROI-wise CBF values, which has been shown in the research setting, but its clinical use remains questionable (92). Because of the relatively large GM/WM CBF contrast, GM atrophy may appear as a CBF decrease, especially given the relatively low spatial resolution of ASL (108). Nevertheless, both GM atrophy and GM CBF reduction will lower the ASL signal and the interaction of both effects may increase the conspicuity of subtle hypoperfusion and may be clinically useful for early detection. However, if GM volume and CBF need to be differentiated in the context of defining early AD biomarkers on a quantitative basis, PVC can be performed to increase the measurement accuracy of GM CBF.

Interpretation

The general approach for using ASL in cerebral neurodegeneration is to search for subtle regional perfusion patterns that associate with specific neurodegenerative processes such as AD, FTD, and DLB. These will almost always be hypoperfusion in general clinical practice. Of note is that patients with MCI and early-stage AD can sometimes present with increased perfusion in the hippocampus and other subcortical regions (potentially attributable to a compensatory mechanism to neuronal injury (109)), though the predominant change seen on a single patient basis will be hypoperfusion. The use of narrow windows and colorized maps is encouraged to increase the conspicuity of these subtle changes (Figure 9). Both aging and neurodegenerative disease can alter macrovascular hemodynamics (110,111) potentially prolonging ATT and thus biasing the CBF measurement. This reduces the sensitivity of ASL for detecting perfusion changes, although it may help identify macrovascular contributions to neurodegenerative pathology (112). White matter CBF may also be a valuable biomarker, as ischemic small vessel disease typically first manifests in the periventricular and subcortical white matter ((113). Although the sensitivity of ASL MRI for quantifying white matter CBF has been controversial (114), the use of higher field strengths (i.e., 3T or higher), background suppression, and optimized labeling durations and PLDs have enabled ASL-based assessment of white matter CBF on an ROI level (115).

Pediatric radiology

Highlights

- Clinical/Physiological
  - ASL in pediatric applications needs adoption from the adult standard
  - Movement in children is more likely and needs to be carefully evaluated
  - Sedation/Anesthesia can influence the CBF
- Sequence

- Smaller voxel size and age-adapted PLD are the foremost considerations
- The choice of single or multi-PLD use is equivalent to adults
- Potential repeated acquisition is a strength of ASL

Indication

ASL is ideal for pediatric cases since it avoids contrast administration and associated challenges of intravenous cannula placement, thus it contributes to the aim of reducing gadolinium use and in further consequence gadolinium accumulation in the body and brain. Furthermore, ASL can even be performed in preterm neonates (116), where gadolinium injection is not FDA-approved (only off-label use is permitted at this time). An additional important advantage of ASL includes instantaneous repeatability in moving infants and children (Figure 10).

Indications for using ASL include the numerous conditions that influence brain perfusion, including tumor monitoring, infections, pediatric stroke (Figure 11), moyamoya, intracranial pressure, and seizures/epilepsy.

Acquisition

Single-PLD PCASL is sufficient for most pediatric applications Since pediatric patients exhibit age-dependent physiological variation related to their developmental stages (such as myelination, hematocrit, brain size, etc.), ASL acquisition parameters should be adapted to the individual age group (Table S3) and physiological factors should also be considered (presented in Table S4). Multi-PLD ASL is indicated in vessel pathologies (117) to estimate ATT and CBF in certain pathologies (e.g. moyamoya), which is often more effective in children compared to adults primarily due to higher cerebral perfusion in children (except infants) (118,119). Dedicated pediatric head coils should be used to maintain SNR, particularly when higher resolution is needed for younger children with smaller brains. In non-sedated children for whom head motion is problematic on conventional sequences, a single-shot 2D EPI sequence can be used in lieu of 3D approaches. Alternatively, image resolution can be lowered to allow for shorter scanning times (13). This is also true for infants examined in the “feed and wrap” technique, as noisy ASL sequences can wake them. Prospective motion correction techniques can be considered (120) and should become available on product sequences in the future. To reduce acquisition time for 3D approaches, the M0 map can be omitted if qualitative evaluation is sufficient.

Post-processing

If absolute CBF quantification is desired, correction for blood T1 variation and hematocrit should be considered if age or disease-related differences are expected, e.g. in anemic patients (121) or neonates (122). However, such corrections will not affect relative measures of perfusion and are difficult to implement in a clinical setting. Cortical thickness decreases (121) and GM-WM CBF ratio changes during brain maturation (119,123). The use of PVC may counteract these effects, but there is no comparative study evaluating PVC effects in children. Alternatives for segmented structural images in PVC are promising, but not yet

clinically established (124). Nevertheless, several pediatric atlases facilitate segmentation in not fully myelinated brains (125–127).

Interpretation

In preterm and term neonates, the CBF of the brainstem, thalami, and basal ganglia as well as sensorimotor cortices is much higher than the rest of the cortex. Special consideration needs to be taken in this group since the development of blood flow and blood volume is heterogeneous (128). Whole-brain CBF generally peaks in preschool children (5–8 years) followed by tapering from childhood to adolescence. Another observation is that the cortical CBF is low in newborns and then increases dramatically to almost double that in the adult brain during the first years of life (129,130). Many of the same disease-specific principles used for analyzing adult ASL data can be applied to pediatric data. It is important to consider that between birth and adulthood, many physiological parameters that may affect CBF measurements will evolve and can also be influenced by disease or sedation (131) (Table S2). Additionally, some sedatives and anesthetics can reduce CBF (e.g. propofol), while others increase CBF (ketamine without benzodiazepine), or have a variable influence on CBF depending on concentration (many narcotic gases) (132). Consideration of all of these factors must be used when interpreting pediatric ASL imaging.

Seizures and Epilepsy

Highlights

- Clinical/Physiological
  - ASL localizes ictal/peri-ictal hyperperfusion and interictal or postictal hypoperfusion
  - Altered regional CBF can drive focused high-resolution imaging to detect small lesions
  - The lack of ionizing radiation allows the use of ASL in each state
- Sequence
  - The single-PLD consensus sequences appears appropriate to be used
  - Relative CBF measures are sufficient for diagnosis
  - Careful labeling planning (and repeatability of positioning) are important factors to distinguish between true or false positives

Indication

Seizure is a common neurological presentation, ranging from a first-time acute seizure to chronic seizure disorders, as seen with epilepsy. Patients are often referred for imaging due to seizures and MRI is often the first choice method to detect structural neocortical lesions (for example, tumors; infectious/inflammatory lesions; encephalomalacia due to prior insult cortical dysplasia, neuronal migration abnormalities, mesial temporal sclerosis, and vascular malformations, amongst other considerations). Conventional MRI findings are unremarkable in 20% to 40% of epilepsy surgery candidates (133). In these cases, functional

neuroimaging techniques, such as PET, SPECT, MEG, and ASL perfusion MRI can reveal the epileptogenic foci (134), with different patterns highlighting the different phases of the disease (e.g., early ictal, ictal, postictal, and interictal) (135). Nevertheless, the use of radiotracers and the high cost of nuclear medicine techniques limit the widespread adoption of these techniques. Because ASL is a repeatable functional technique with no radiation exposure or contrast injection, it can be easily acquired in conjunction with structural MRI to detect areas of abnormal perfusion that may corroborate and/or complement electroencephalogram (EEG) and clinical findings. Such results can potentially direct further investigation into brain regions that should be imaged using additional high-resolution structural sequences. Seizures or epilepsy often manifest in ASL as either ictal or peri-ictal hyperperfusion or as postictal or interictal (Figure 12) hypoperfusion.

Acquisition

Single-PLD ASL using the recommended consensus parameters is sufficient for evaluating seizures and searching for epileptogenic foci. Since seizure and epilepsy are not expected to systematically modulate arterial transit times, multi-PLD acquisitions are not necessary and do not improve the detection of brain perfusion alteration.

Post-Processing

Visual evaluation of simple control-label subtraction images (136) for hemispheric perfusion symmetry is the first and fundamental step for an adequate clinical evaluation (Figure 13). Absolute CBF quantification is not typically required for diagnosis. However, an important approach is the evaluation of images based on asymmetry indices, which are calculated in or near the epileptic focus relative to the contralateral normal-appearing tissue (135,137).

Interpretation

Searching for focal areas of CBF asymmetry between the two cerebral hemispheres forms the mainstay for evaluation; this must take into account both the clinical and EEG findings and the potential occurrence of coexisting intracranial vascular abnormalities or abnormalities of another origin. If flow asymmetry is correlated with the clinical/EEG foci, this may be due to either an increase in perfusion associated with the epileptogenic focus (e.g. in the ictal phase) or to its reduction (in the interictal phase). It is important also to recognize that hemispheric or territorial asymmetries in ASL can arise from differential labeling efficiency due to various factors (e.g. vessel geometry and/or tortuosity) correlation with MRA or contrast perfusion (if available) can be helpful to identify false-positive results. Repeat studies with repositioning of the labeling plane can also be considered in ambiguous cases.

Standard Interpretation and Reporting

Standardized reporting may not only aid radiologists, but also help the referring clinicians to better understand the interpretation of an ASL scan. Before the radiological/clinical interpretation of an ASL image, quality control should be performed to ensure its diagnostic quality, particularly since the physiological nature of ASL and its relatively low signal-to-noise ratio makes the technique sensitive to both technical and physiological artifacts.

Moreover, these may not always be immediately obvious to the non-expert reader. Before interpreting ASL images, the reader is encouraged to evaluate and report the following criteria:

- Overall image quality: Is the SNR as expected, and is the cortex visible and well-defined? Is there any subtle patient motion that could corrupt the image or lead to false positives or negatives?
- Symmetry: Is the perfusion distribution symmetrical? If not: Does the clinical question explain any asymmetries in perfusion? Does the asymmetry follow a vascular territory, which could reflect a true perfusion abnormality or related to asymmetric labeling efficiency (very common between the cervical internal carotid and vertebral arteries)? When performing PCASL it can be valuable to plan the ASL on sagittal and coronal angiography surveys (for example, if the patient has already had an MRA) such that the labeling plane is roughly perpendicular to both the internal carotid and vertebral arteries.
- Labeling: In ASL, the problem can lie outside the field of view, e.g., labeling may be degraded in patients with dental implants and/or carotid stents and can lead to misinterpretation (138). On single-delay ASL scans, a unilateral fetal variant of the posterior cerebral artery (PCA) can create the image of apparent (or pseudo-) hypoperfusion in the contralateral PCA territory. Similarly, when both PCAs have a regular (non-hypoplastic) P1 segment and there is not a significant contribution of the posterior communicating artery blood flow, both posterior cerebral artery territories can demonstrate pseudo-hypoperfusion relative to the anterior circulation territories. This is a result of hemodynamic differences between the carotid and vertebrobasilar arteries (that can be more pronounced in older patients) and should not be misinterpreted as true hypoperfusion (139).
- Hyperintensities: Check for vascularly shaped (focal curvilinear or round foci) with extreme perfusion values, a.k.a. ATA. If ATAs are affecting all territories, are there physiological reasons for the patient to have global transit delays, such as decreased ejection fraction/cardiac output or advanced age? Or is it fitting with age? If it affects only a single region/territory, check for stenosis or collateral arteries. If located in large veins, can they be physiological (micro-shunting) or anatomical (macro-shunting)? See the AVM section for details.
- Feedback: Is there any feedback from the technicians who have performed the acquisition (movement, planning difficulties, lack of cooperation, etc.); Check cuff position in intubated children is not at labeling level
- Parameters: Is the information that I have complete? (necessary parameters are listed in table 1)

It should be stressed that many ASL images will be less than perfect, just as is the case with structural imaging. However, if the perfusion signal is realistic and consistent with what is expected based on physiology or pathophysiology, the scan is likely of diagnostic quality.

Required technical information for the radiologist

The labeling duration, labeling plane position (in PCASL), and PLDs are the most essential pieces of information to be able to interpret the (quantified) CBF image. In the case of multi-PLD ASL, the different delay times need to be taken into account as well. Other information may be important in special diseases and can be viewed as optional. This includes the use of vascular crushing or background suppression. Pre-existing conditions are known to influence CBF, either whole-brain (neurodegeneration), focal (tumors, stenosis) or systemic (SCA) or use of vasoactive medication or caffeine (if possible to evaluate) before the scan, are important to be taken into account as well.

Furthermore, any deviations from the original protocol need to be communicated, e.g. “adapted for pediatrics” or “expected longer ATT and increased PLD” if the technologists are expected to run alternative ASL versions instead of the standard protocol.

Discussion

Despite the great number of technical advances in ASL over the past several years, the 2015 consensus recommendations are still appropriate for many clinical indications. This is especially the case when aiming for a “one-fits-all” sequence in keeping with the standard single-PLD 3D PCASL sequence from the previous consensus paper, ideally with age-adapted PLD. Subtle protocol modifications of the recommended PCASL sequence may help in certain disease areas, especially in conditions presenting significant variability of hemodynamics. The main use-case of ASL is adding a physiological perspective without external contrast agent usage to neurological diseases, which are in most cases vascular or at least have a vascular component.

The main reason to adapt ASL to a certain disease lies within the complexity of the ASL signal, which can have both a macrovascular and tissue perfusion component. Many studies and clinical experience have shown that the 2015 consensus PLD of 1800–2000 ms may not be sufficient for all the labeled blood to arrive in the brain parenchyma, especially in cases of vascular compromise, which is common in both normal and abnormal aging. Even though multi-PLD can improve the diagnostic accuracy of ASL, in many clinical cases, there is still a lack of availability of this sequence and its post-processing on clinical scanners. Also, multi-PLD can require scanning times that are clinically not feasible and can be more sensitive to motion than a single-PLD ASL sequence. Therefore, single-PLD is still seen as the default clinical ASL sequence, similar to the 2015 consensus. Multi-PLD ASL on the other hand is particularly helpful in diseases with delayed arterial transit times such as AIS and SOD, as single PLD approaches will not be able to accurately quantify CBF in regions affected by this delay. Furthermore, multi-PLD allows the generation of an ATT map. If this is not available, a long label, long PLD approach, or a two-PLD scheme can be used as an alternative.

Often, users are limited in their freedom of modifying ASL product sequences, which could make them unable to apply certain recommendations. In these cases, the 2015 recommendation, as implemented by most vendors, is still adequate, though careful attention

should be paid to the potential pitfalls of these parameters. We hope that some of these more specialized methods could be adopted in subsequent vendor products given their potential value, particularly motion correction and robustness to off-resonance effects in the brain and for labeling. Readers are encouraged to obtain detailed knowledge about their available ASL sequence from the vendor, as well as options to modify the sequence for special needs. While the main focus lies on the use in clinical routine, these consensus recommendations can also be used as guidance for clinical research studies of subtypes of the presented diseases. This guidance paper did not include, as of today, novel developments such as VSASL, BBB-ASL, etc. due to the lack of clinical experience and availability of product sequences. Such advanced ASL techniques can be expected to play a prominent role in future perfusion imaging of various pathologies, e.g. tumors (140). Of special concern here is VSASL, which is expected to be beneficial in cases of prolonged ATT. Another consensus recommendation paper on this topic is part of the current effort of harmonizing ASL. Also, we did not address subtypes of diseases, e.g. mild cognitive impairment, bipolar disorder, or depression. We hope that the present guidance on specific diseases will take away the guesswork and uncertainty for radiologists to implement ASL more frequently, assisting those who intend to use ASL on a single-patient basis.

Supplementary Material

Refer to Web version on PubMed Central for supplementary material.

Acknowledgments

HM, FB, VK, and MG are supported by the Eurostars-2 joint program with co-funding from the European Union Horizon 2020 research and innovation program (ASPIRE E!113701), provided by the Netherlands Enterprise Agency (RvO). HM and JP are supported by the Dutch Heart Foundation (2020T049). HM, JP, MG, and EA are supported by the EU Joint Program for Neurodegenerative Disease Research, provided by the Netherlands Organization for Health Research and Development and Alzheimer Nederland (DEBBIE JPND2020-568-106). TL is supported by the German Research Foundation (DFG) grant number LI-3030/2-1. FB, XG are supported by the National Institute of Health Research Biomedical Research Centre at UCLH. HK is supported by a scientific research grant from Japan Society for the Promotion of Science (2 1 K 0 7 6 1 6). MRJ is supported by the American Heart Association (19CDA34790002) and by the National Institutes of Health/National Institute on Aging (1K01AG070318). XL is supported by grants from the National Natural Science Foundation of China (nos. 81825012,81730048 and 82151309). NP is funded by the Dent Family Foundation.

Funding information

We did not obtain specific funding for writing this guidance paper.

Disclosure

DJW is a shareholder of Translational MRI, LLC. XG is founder, shareholder and CEO of Gold Standard Phantoms Ltd. MG is founder of mediri Gmbh and Deputy director of Fraunhofer MEVIS. FB serves on trial steering/safety committees for Biogen, Merck, Roche, EISAI. He is a consultant for Roche, Biogen, Merck, IXICO, Jansen, Combinostics and has research agreements with Novartis, Merck, Biogen, GE and Roche. He is co-founder and shareholder of Queen Square Analytics LTD. MS discloses receipt of speaker fees (paid to institution) from GE Healthcare. GZ is co-founder of Subtle Medical, in the advisory board of Biogen and received research funding from GE Healthcare. DB received a GE Healthcare Industry-supported research grant. MH received grants from RSNA/Siemens Healthineers Research Scholar Grant, Italfarmaco ImagingDMD Grant, Bayer Healthcare Radiology Medical Education Grant and Cardinal Health Foundation Research Grant.

List of abbreviations

AD	Alzheimer Disease

ASL	Arterial Spin Labeling
AIS	Acute Ischemic Stroke
ATA	Arterial Transit Artifact
ATT	Arterial Transit Time
AVF	Arteriovenous Fistula
AVM	Arteriovenous Malformation
BBB	Blood Brain Barrier
CBF	Cerebral Blood Flow
CTA	Computed Tomography Angiography
DSC	Dynamic Susceptibility Contrast
DVA	Developmental Venous Anomaly
EEG	Electroencephalogram
EPI	Echo Planar Imaging
FTD	Frontotemporal Dementia
GraSE	Gradient Spin Echo
GM	Gray Matter
MCI	Mild Cognitive Impairment
MRA	Magnetic Resonance Angiography
MRI	Magnetic Resonance Imaging
PCASL	Pseudo-continuous Arterial Spin Labeling
PET	Positron Emission Tomography
PLD	Post Labeling Delay
PVC	Partial Volume Correction
SOD	Steno-occlusive Disease
SPECT	Single Photon Computed Tomography
TVA	Transitional Venous Anomaly
VSASL	Velocity-selective Arterial Spin Labeling
WM	White Matter

Reference list

1. Haller S, Zaharchuk G, Thomas DL, Lovblad K-O, Barkhof F, Golay X. Arterial Spin Labeling Perfusion of the Brain : Emerging Clinical Applications. Radiology 2016;281:337–356. [PubMed: 27755938]
2. Grade M, Hernandez Tamames JA, Pizzini FB, Achten E, Golay X, Smits M. A neuroradiologist's guide to arterial spin labeling MRI in clinical practice. Neuroradiology 2015;57:1181–1202. [PubMed: 26351201]
3. Deibler AR, Pollock JM, Kraft RA, Tan H, Burdette JH, Maldjian JA. Arterial spin-labeling in routine clinical practice, part 2: hypoperfusion patterns. AJNR Am.J.Neuroradiol 2008;29:1235–1241. [PubMed: 18356467]
4. Deibler AR, Pollock JM, Kraft RA, Tan H, Burdette JH, Maldjian JA. Arterial spin-labeling in routine clinical practice, part 3: hyperperfusion patterns. AJNR Am.J.Neuroradiol 2008;29:1428–1435. [PubMed: 18356466]
5. van der Plas MCE, Teeuwisse WM, Schmid S, Chappell M, van Osch MJP. High temporal resolution arterial spin labeling MRI with whole-brain coverage by combining time-encoding with Look-Locker and simultaneous multi-slice imaging. Magn. Reson. Med 2019;81:3734–3744. [PubMed: 30828873]
6. Sugimori H, Fujima N, Suzuki Y, Hamaguchi H, Sakata M, Kudo K. Evaluation of cerebral blood flow using multi-phase pseudo continuous arterial spin labeling at 3-tesla. Magn. Reson. Imaging 2015;33:1338–1344. [PubMed: 26260545]
7. Mutsaerts HJMM, Petr J, Groot P, et al. ExploreASL: An image processing pipeline for multi-center ASL perfusion MRI studies. Neuroimage 2020;219:117031. [PubMed: 32526385]
8. Warnert EAH, Steketee RME, Vernooij MW, et al. Implementation and validation of ASL perfusion measurements for population imaging. Magn. Reson. Med 2020;84:2048–2054. [PubMed: 32239745]
9. Pinto J, Chappell MA, Okell TW, et al. Calibration of arterial spin labeling data-potential pitfalls in post-processing. Magn. Reson. Med 2019 doi: 10.1002/mrm.28000.
10. Shirzadi Z, Stefanovic B, Chappell MA, et al. Enhancement of automated blood flow estimates (ENABLE) from arterial spin-labeled MRI. J. Magn. Reson. Imaging 2018;47:647–655. [PubMed: 28681479]
11. Wu MM, Chan S-T, Mazumder D, et al. Improved accuracy of cerebral blood flow quantification in the presence of systemic physiology cross-talk using multi-layer Monte Carlo modeling. Neurophotonics 2021;8:015001. [PubMed: 33437846]
12. Wong EC, Cronin M, Wu W-C, Inglis B, Frank LR, Liu TT. Velocity-selective arterial spin labeling. Magn. Reson. Med 2006;55:1334–1341. [PubMed: 16700025]
13. Alsop DC, Detre JA, Golay X, et al. Recommended implementation of arterial spin-labeled perfusion MRI for clinical applications: A consensus of the ISMRM perfusion study group and the european consortium for ASL in dementia. Magnetic Resonance in Medicine 2014 doi: 10.1002/mrm.25197.
14. Vidorreta M, Balteau E, Wang Z, et al. Evaluation of segmented 3D acquisition schemes for whole-brain high-resolution arterial spin labeling at 3 T. NMR Biomed. 27:1387–1396.
15. Petr J, Mutsaerts HJMM, De Vita E, et al. Effects of systematic partial volume errors on the estimation of gray matter cerebral blood flow with arterial spin labeling MRI. MAGMA 2018;31:725–734. [PubMed: 29916058]
16. Ssali T, Anazodo UC, Narciso L, et al. Sensitivity of arterial Spin labeling for characterization of longitudinal perfusion changes in Frontotemporal dementia and related disorders. Neuroimage Clin 2021:102853. [PubMed: 34697009]
17. Zhao L, Vidorreta M, Soman S, Detre JA, Alsop DC. Improving the robustness of pseudo-continuous arterial spin labeling to off-resonance and pulsatile flow velocity. Magn. Reson. Med 2017;78:1342–1351. [PubMed: 27774656]
18. Clement P, Mutsaerts H, Vaclavu L, et al. Variability of physiological brain perfusion in healthy subjects - A systematic review of modifiers. Considerations for multi-center ASL studies. J. Cereb. Blood Flow Metab 2017;In press doi: 10.1177/0271678X17702156.

19. Haller S, Rodriguez C, Moser D, et al. Acute caffeine administration impact on working memory-related brain activation and functional connectivity in the elderly: a BOLD and perfusion MRI study. Neuroscience 2013;250:364–371. [PubMed: 23876323]
20. Haller S, Montandon M-L, Rodriguez C, et al. Acute caffeine administration effect on brain activation patterns in mild cognitive impairment. J. Alzheimers. Dis 2014;41:101–112. [PubMed: 24577471]
21. Bokkers RPH, Bremmer JP, van Berckel BNM, et al. Arterial spin labeling perfusion MRI at multiple delay times: a correlative study with H(2)(15)O positron emission tomography in patients with symptomatic carotid artery occlusion. J. Cereb. Blood Flow Metab 2010;30:222–229. [PubMed: 19809464]
22. Jezzard P, Chappell MA, Okell TW. Arterial spin labeling for the measurement of cerebral perfusion and angiography. J. Cereb. Blood Flow Metab 2018;38:603–626. [PubMed: 29168667]
23. Wang, Alger, Qiao, Gunther, Pope. Multi-delay multi-parametric arterial spin-labeled perfusion MRI in acute ischemic stroke—comparison with dynamic susceptibility contrast enhanced …. NeuroImage Clin.
24. Van Der Thiel Rodriguez. Brain perfusion measurements using multidelay arterial spin-labeling are systematically biased by the number of delays. Am. J. Physiol. Renal Physiol
25. Heijtel DFR, Mutsaerts HJMM, Bakker E, et al. Accuracy and precision of pseudo-continuous arterial spin labeling perfusion during baseline and hypercapnia: a head-to-head comparison with ^{15}O H_2O positron emission tomography. Neuroimage 2014;92:182–192. [PubMed: 24531046]
26. Chen Z, Zhang X, Yuan C, Zhao X, van Osch MJP. Measuring the labeling efficiency of pseudocontinuous arterial spin labeling. Magn. Reson. Med 2017;77:1841–1852. [PubMed: 27174204]
27. Hales PW, Kirkham FJ, Clark CA. A general model to calculate the spin-lattice (T1) relaxation time of blood, accounting for haematocrit, oxygen saturation and magnetic field strength. J.Cereb.Blood Flow Metab 2016;36:370–374. [PubMed: 26661147]
28. Roach BA, Donahue MJ, Davis LT, et al. Interrogating the Functional Correlates of Collateralization in Patients with Intracranial Stenosis Using Multimodal Hemodynamic Imaging. AJNR Am. J. Neuroradiol 2016;37:1132–1138. [PubMed: 27056428]
29. Zaharchuk G, Do HM, Marks MP, Rosenberg J, Moseley ME, Steinberg GK. Arterial spin-labeling MRI can identify the presence and intensity of collateral perfusion in patients with moyamoya disease. Stroke 2011;42:2485–2491. [PubMed: 21799169]
30. Pinter NK, Fritz JV. Neuroimaging for the Neurologist: Clinical MRI and Future Trends. Neurol. Clin 2020;38:1–35. [PubMed: 31761054]
31. Fan AP, Guo J, Khalighi MM, et al. Long-Delay Arterial Spin Labeling Provides More Accurate Cerebral Blood Flow Measurements in Moyamoya Patients: A Simultaneous Positron Emission Tomography/MRI Study. Stroke 2017;48:2441–2449. [PubMed: 28765286]
32. Lou X, Ma X, Liebeskind DS, et al. Collateral perfusion using arterial spin labeling in symptomatic versus asymptomatic middle cerebral artery stenosis. J. Cereb. Blood Flow Metab 2019;39:108–117. [PubMed: 28786338]
33. Lyu J, Ma N, Liebeskind DS, et al. Arterial Spin Labeling Magnetic Resonance Imaging Estimation of Antegrade and Collateral Flow in Unilateral Middle Cerebral Artery Stenosis. Stroke 2016;47:428–433. [PubMed: 26732570]
34. Buxton RB, Frank LR, Wong EC, Siewert B, Warach S, Edelman RR. A general kinetic model for quantitative perfusion imaging with arterial spin labeling. Magn. Reson. Med 1998;40:383–396. [PubMed: 9727941]
35. Wang DJJ, Alger JR, Qiao JX, et al. Multi-delay multi-parametric arterial spin-labeled perfusion MRI in acute ischemic stroke - Comparison with dynamic susceptibility contrast enhanced perfusion imaging. Neuroimage Clin 2013;3:1–7. [PubMed: 24159561]
36. Bokkers RPH, Hernandez DA, Merino JG, et al. Whole-brain arterial spin labeling perfusion MRI in patients with acute stroke. Stroke 2012;43:1290–1294. [PubMed: 22426319]
37. Zaharchuk G, El Mogy IS, Fischbein NJ, Albers GW. Comparison of arterial spin labeling and bolus perfusion-weighted imaging for detecting mismatch in acute stroke. Stroke 2012;43:1843–1848. [PubMed: 22539548]

38. Wang DJJ, Alger JR, Qiao JX, et al. The value of arterial spin-labeled perfusion imaging in acute ischemic stroke: comparison with dynamic susceptibility contrast-enhanced MRI. Stroke 2012;43:1018–1024. [PubMed: 22328551]
39. Nogueira RG, Jadhav AP, Haussen DC, et al. Thrombectomy 6 to 24 Hours after Stroke with a Mismatch between Deficit and Infarct. N. Engl. J. Med 2018;378:11–21. [PubMed: 29129157]
40. Albers GW, Marks MP, Kemp S, et al. Thrombectomy for Stroke at 6 to 16 Hours with Selection by Perfusion Imaging. N. Engl. J. Med 2018;378:708–718. [PubMed: 29364767]
41. de Havenon A, Haynor DR, Tirschwell DL, et al. Association of Collateral Blood Vessels Detected by Arterial Spin Labeling Magnetic Resonance Imaging With Neurological Outcome After Ischemic Stroke. JAMA Neurol. 2017;74:453–458. [PubMed: 28192548]
42. De Vis JB, Alderliesten T, Hendrikse J, Petersen ET, Benders MJNL. Magnetic resonance imaging based noninvasive measurements of brain hemodynamics in neonates: a review. Pediatr. Res 2016;80:641–650. [PubMed: 27434119]
43. Le TT, Fischbein NJ, Andre JB, Wijman C, Rosenberg J, Zaharchuk G. Identification of venous signal on arterial spin labeling improves diagnosis of dural arteriovenous fistulas and small arteriovenous malformations. AJNR Am. J. Neuroradiol 2012;33:61–68. [PubMed: 22158927]
44. Togao O, Hiwatashi A, Obara M, et al. Acceleration-selective Arterial Spin-labeling MR Angiography Used to Visualize Distal Cerebral Arteries and Collateral Vessels in Moyamoya Disease. Radiology 2018;286:611–621. [PubMed: 28915102]
45. Morofuji Y, Horie N, Tateishi Y, et al. Arterial Spin Labeling Magnetic Resonance Imaging Can Identify the Occlusion Site and Collateral Perfusion in Patients with Acute Ischemic Stroke: Comparison with Digital Subtraction Angiography. Cerebrovasc. Dis 2019;48:70–76. [PubMed: 31553986]
46. Bivard A, Krishnamurthy V, Stanwell P, et al. Arterial spin labeling versus bolus-tracking perfusion in hyperacute stroke. Stroke 2014;45:127–133. [PubMed: 24302482]
47. Yu S, Liebeskind DS, Dua S, et al. Postischemic hyperperfusion on arterial spin labeled perfusion MRI is linked to hemorrhagic transformation in stroke. J. Cereb. Blood Flow Metab 2015;35:630–637. [PubMed: 25564233]
48. Okazaki S, Yamagami H, Yoshimoto T, et al. Cerebral hyperperfusion on arterial spin labeling MRI after reperfusion therapy is related to hemorrhagic transformation. J. Cereb. Blood Flow Metab 2017;37:3087–3090. [PubMed: 28665168]
49. Lee S, Park DW, Kim TY, et al. A novel visual ranking system based on arterial spin labeling perfusion imaging for evaluating perfusion disturbance in patients with ischemic stroke. PLoS One 2020;15:e0227747. [PubMed: 31978097]
50. Bolar DS, Gagoski B, Orbach DB, et al. Comparison of CBF Measured with Combined Velocity-Selective Arterial Spin-Labeling and Pulsed Arterial Spin-Labeling to Blood Flow Patterns Assessed by Conventional Angiography in Pediatric Moyamoya. AJNR Am. J. Neuroradiol 2019;40:1842–1849. [PubMed: 31694821]
51. Qiu D, Straka M, Zun Z, Bammer R, Moseley ME, Zaharchuk G. CBF measurements using multidelay pseudocontinuous and velocity-selective arterial spin labeling in patients with long arterial transit delays: comparison with xenon CT CBF. J. Magn. Reson. Imaging 2012;36:110–119. [PubMed: 22359345]
52. Di Napoli A, Cheng SF, Gregson J, et al. Arterial Spin Labeling MRI in Carotid Stenosis: Arterial Transit Artifacts May Predict Symptoms. Radiology 2020;297:652–660. [PubMed: 33048034]
53. Donahue MJ, Dethrage LM, Faraco CC, et al. Routine clinical evaluation of cerebrovascular reserve capacity using carbogen in patients with intracranial stenosis. Stroke 2014;45:2335–2341. [PubMed: 24938845]
54. Hodel J, Leclerc X, Kalsoum E, et al. Intracranial Arteriovenous Shunting: Detection with Arterial Spin-Labeling and Susceptibility-Weighted Imaging Combined. AJNR Am. J. Neuroradiol 2017;38:71–76. [PubMed: 27789452]
55. Wolf RL, Wang J, Detre JA, Zager EL, Hurst RW. Arteriovenous shunt visualization in arteriovenous malformations with arterial spin-labeling MR imaging. AJNR Am. J. Neuroradiol 2008;29:681–687. [PubMed: 18397967]

56. Heit JJ, Thakur NH, Iv M, et al. Arterial-spin labeling MRI identifies residual cerebral arteriovenous malformation following stereotactic radiosurgery treatment. J. Neuroradiol 2020;47:13–19. [PubMed: 30658138]
57. Sunwoo L, Sohn C-H, Lee JY, et al. Evaluation of the degree of arteriovenous shunting in intracranial arteriovenous malformations using pseudo-continuous arterial spin labeling magnetic resonance imaging. Neuroradiology 2015;57:775–782. [PubMed: 25903432]
58. Amponsah K, Ellis TL, Chan MD, et al. Retrospective analysis of imaging techniques for treatment planning and monitoring of obliteration for gamma knife treatment of cerebral arteriovenous malformation. Neurosurgery 2012;71:893–899. [PubMed: 22791027]
59. Suazo L, Foerster B, Fermin R, et al. Measurement of blood flow in arteriovenous malformations before and after embolization using arterial spin labeling. Interv. Neuroradiol 2012;18:42–48. [PubMed: 22440600]
60. Blauwblomme T, Naggara O, Brunelle F, et al. Arterial spin labeling magnetic resonance imaging: toward noninvasive diagnosis and follow-up of pediatric brain arteriovenous malformations. J. Neurosurg. Pediatr 2015;15:451–458. [PubMed: 25634818]
61. Pollock JM, Whitlow CT, Simonds J, et al. Response of arteriovenous malformations to gamma knife therapy evaluated with pulsed arterial spin-labeling MRI perfusion. AJR Am. J. Roentgenol 2011;196:15–22. [PubMed: 21178042]
62. Iv M, Fischbein NJ, Zaharchuk G. Association of developmental venous anomalies with perfusion abnormalities on arterial spin labeling and bolus perfusion-weighted imaging. J. Neuroimaging 2015;25:243–250. [PubMed: 24717021]
63. Juttukonda MR, Donahue MJ, Davis LT, et al. Preliminary evidence for cerebral capillary shunting in adults with sickle cell anemia. Journal of Cerebral Blood Flow & Metabolism 2019;39:1099–1110 doi: 10.1177/0271678x17746808. [PubMed: 29260615]
64. Bush A, Chai Y, Choi SY, et al. Pseudo continuous arterial spin labeling quantification in anemic subjects with hyperemic cerebral blood flow. Magn. Reson. Imaging 2018;47:137–146. [PubMed: 29229306]
65. Juttukonda MR, Donahue MJ, Waddle SL, et al. Reduced oxygen extraction efficiency in sickle cell anemia patients with evidence of cerebral capillary shunting. J. Cereb. Blood Flow Metab 2021;41:546–560. [PubMed: 32281458]
66. Falk Delgado A, De Luca F, van Westen D, Falk Delgado A. Arterial spin labeling MR imaging for differentiation between high- and low-grade glioma-a meta-analysis. Neuro. Oncol 2018;20:1450–1461. [PubMed: 29868920]
67. Dangouloff-Ros V, Deroulers C, Foissac F, et al. Arterial Spin Labeling to Predict Brain Tumor Grading in Children: Correlations between Histopathologic Vascular Density and Perfusion MR Imaging. Radiology 2016;281:553–566. [PubMed: 27257950]
68. Smits M MRI biomarkers in neuro-oncology. Nat. Rev. Neurol 2021 doi: 10.1038/s41582-021-00510-y.
69. Sunwoo L, Yun TJ, You S-H, et al. Differentiation of Glioblastoma from Brain Metastasis: Qualitative and Quantitative Analysis Using Arterial Spin Labeling MR Imaging. PLoS One 2016;11:e0166662. [PubMed: 27861605]
70. Weber MA, Zoubaa S, Schlieter M, et al. Diagnostic performance of spectroscopic and perfusion MRI for distinction of brain tumors. Neurology 2006;66:1899–1906. [PubMed: 16801657]
71. Suh CH, Kim HS, Jung SC, Choi CG, Kim SJ. Perfusion MRI as a diagnostic biomarker for differentiating glioma from brain metastasis: a systematic review and meta-analysis. Eur. Radiol 2018;28:3819–3831. [PubMed: 29619517]
72. Alsaedi A, Doniselli F, Jäger HR, et al. The value of arterial spin labelling in adults glioma grading: systematic review and meta-analysis. Oncotarget 2019;10:1589–1601. [PubMed: 30899427]
73. Choi YJ, Kim HS, Jahng G-H, Kim SJ, Suh DC. Pseudoprogression in patients with glioblastoma: added value of arterial spin labeling to dynamic susceptibility contrast perfusion MR imaging. Acta radiol. 2013;54:448–454. [PubMed: 23592805]

74. Manning P, Daghighi S, Rajaratnam MK, et al. Differentiation of progressive disease from pseudoprogression using 3D PCASL and DSC perfusion MRI in patients with glioblastoma. J. Neurooncol 2020;147:681–690. [PubMed: 32239431]

75. Maral H, Ertekin E, Tunçyürek Ö, Özsunar Y. Effects of Susceptibility Artifacts on Perfusion MRI in Patients with Primary Brain Tumor: A Comparison of Arterial Spin-Labeling versus DSC. AJNR Am. J. Neuroradiol 2020;41:255–261. [PubMed: 31974077]

76. Yang S, Zhao B, Wang G, et al. Improving the Grading Accuracy of Astrocytic Neoplasms Noninvasively by Combining Timing Information with Cerebral Blood Flow: A Multi-TI Arterial Spin-Labeling MR Imaging Study. AJNR Am. J. Neuroradiol 2016;37:2209–2216. [PubMed: 27561831]

77. Crameri F, Shephard GE, Heron PJ. The misuse of colour in science communication. Nat. Commun 2020;11:5444. [PubMed: 33116149]

78. Zabala-Travers S, Choi M, Cheng W-C, Badano A. Effect of color visualization and display hardware on the visual assessment of pseudocolor medical images. Med. Phys 2015;42:2942–2954. [PubMed: 26127048]

79. Andre JB, Nagpal S, Hippe DS, et al. Cerebral Blood Flow Changes in Glioblastoma Patients Undergoing Bevacizumab Treatment Are Seen in Both Tumor and Normal Brain. Neuroradiol. J 2015;28:112–119. [PubMed: 25923677]

80. Petr J, Platzek I, Hofheinz F, et al. Photon vs. proton radiochemotherapy, effects on brain tissue volume and perfusion. Radiother. Oncol 2018;In press doi: 10.1016/j.radonc.2017.11.033.

81. Sandson TA, O'Connor M, Sperling RA, Edelman RR, Warach S. Noninvasive perfusion MRI in Alzheimer's disease: a preliminary report. Neurology 1996;47:1339–1342. [PubMed: 8909457]

82. Alsop DC, Detre JA, Grossman M. Assessment of cerebral blood flow in Alzheimer's disease by spin-labeled magnetic resonance imaging. Ann.Neurol 2000;47:93–100. [PubMed: 10632106]

83. Binnewijzend MAA, Kuijer JPA, Benedictus MR, et al. Cerebral blood flow measured with 3D pseudocontinuous arterial spin-labeling MR imaging in Alzheimer disease and mild cognitive impairment: a marker for disease severity. Radiology 2013;267:221–230. [PubMed: 23238159]

84. Johnson NA, Jahng GH, Weiner MW, et al. Pattern of cerebral hypoperfusion in Alzheimer disease and mild cognitive impairment measured with arterial spin-labeling MR imaging: initial experience. Radiology 2005;234:851–859. [PubMed: 15734937]

85. Tosun D, Schuff N, Rabinovici GD, et al. Diagnostic utility of ASL-MRI and FDG-PET in the behavioral variant of FTD and AD. Ann Clin Transl Neurol 2016;3:740–751. [PubMed: 27752510]

86. Dai W, Lopez OL, Carmichael OT, Becker JT, Kuller LH, Gach HM. Mild cognitive impairment and alzheimer disease: patterns of altered cerebral blood flow at MR imaging. Radiology 2009;250:856–866. [PubMed: 19164119]

87. Alsop DC, Casement M, De BC, Fong T, Press DZ. Hippocampal hyperperfusion in Alzheimer's disease. Neuroimage 2008;42:1267–1274. [PubMed: 18602481]

88. Hu WT, Wang Z, Lee VM, Hu WT, Lee VM. Distinct cerebral perfusion patterns in FTLD and AD. 2011 doi: 10.1212/WNL.0b013e3181f11e35.

89. Asllani I, Habeck C, Scarmeas N, Borogovac A, Brown TR, Stern Y. Multivariate and univariate analysis of continuous arterial spin labeling perfusion MRI in Alzheimer's disease. J.Cereb.Blood Flow Metab 2008;28:725–736. [PubMed: 17960142]

90. Chao LL, Buckley ST, Kornak J, et al. ASL perfusion MRI predicts cognitive decline and conversion from MCI to dementia. Alzheimer Dis.Assoc.Disord 2010;24:19–27. [PubMed: 20220321]

91. Mutsaerts HJMM, Mirza SS, Petr J, et al. Cerebral perfusion changes in presymptomatic genetic frontotemporal dementia: a GENFI study. Brain 2019;142:1108–1120. [PubMed: 30847466]

92. Dolui S, Li Z, Nasrallah IM, Detre JA, Wolk DA. Arterial spin labeling versus F-FDG-PET to identify mild cognitive impairment. Neuroimage Clin 2020;25:102146. [PubMed: 31931403]

93. Nedelska Z, Senjem ML, Przybelski SA, et al. Regional cortical perfusion on arterial spin labeling MRI in dementia with Lewy bodies: Associations with clinical severity, glucose metabolism and tau PET. Neuroimage Clin 2018;19:939–947. [PubMed: 30003031]

94. Kamagata K, Motoi Y, Hori M, et al. Posterior hypoperfusion in Parkinson's disease with and without dementia measured with arterial spin labeling MRI. J.Magn Reson.Imaging 2011;33:803–807. [PubMed: 21448943]
95. Fällmar D, Haller S, Lilja J, et al. Arterial spin labeling-based Z-maps have high specificity and positive predictive value for neurodegenerative dementia compared to FDG-PET. Eur. Radiol 2017;27:4237–4246. [PubMed: 28374078]
96. Steketee RME, Bron EE, Meijboom R, et al. Early-stage differentiation between presenile Alzheimer's disease and frontotemporal dementia using arterial spin labeling MRI. Eur. Radiol 2016;26:244–253. [PubMed: 26024845]
97. Du AT, Jahng GH, Hayasaka S, et al. Hypoperfusion in frontotemporal dementia and Alzheimer disease by arterial spin labeling MRI. Neurology 2006;67:1215–1220. [PubMed: 17030755]
98. Mak E, Dounavi M-E, Low A, et al. Proximity to dementia onset and multi-modal neuroimaging changes: The prevent-dementia study. Neuroimage 2021;229:117749. [PubMed: 33454416]
99. Li D, Liu Y, Zeng X, et al. Quantitative Study of the Changes in Cerebral Blood Flow and Iron Deposition During Progression of Alzheimer's Disease. J. Alzheimers. Dis 2020;78:439–452. [PubMed: 32986675]
100. Kim SM, Kim MJ, Rhee HY, et al. Regional cerebral perfusion in patients with Alzheimer's disease and mild cognitive impairment: effect of APOE epsilon4 allele. Neuroradiology 2013;55:25–34. [PubMed: 22828738]
101. Xekardaki A, Rodriguez C, Montandon M-L, et al. Arterial spin labeling may contribute to the prediction of cognitive deterioration in healthy elderly individuals. Radiology 2015;274:490–499. [PubMed: 25291458]
102. Brendel M, Barthel H, van Eimeren T, et al. Assessment of 18F-PI-2620 as a Biomarker in Progressive Supranuclear Palsy. JAMA Neurol. 2020;77:1408–1419. [PubMed: 33165511]
103. Gorelick PB, Scuteri A, Black SE, et al. Vascular contributions to cognitive impairment and dementia: a statement for healthcare professionals from the american heart association/american stroke association. Stroke 2011;42:2672–2713. [PubMed: 21778438]
104. Simão F, Pagnussat AS, Seo JH, et al. Pro-angiogenic effects of resveratrol in brain endothelial cells: nitric oxide-mediated regulation of vascular endothelial growth factor and metalloproteinases. J. Cereb. Blood Flow Metab 2012;32:884–895. [PubMed: 22314268]
105. Aoike S, Sugimori H, Fujima N, et al. Three-dimensional Pseudo-continuous Arterial Spin-labeling Using Turbo-spin Echo with Pseudo-steady State Readout: A Comparison with Other Major Readout Methods. Magn. Reson. Med. Sci 2019;18:170–177. [PubMed: 30318501]
106. Spiral imaging in fMRI. Neuroimage 2012;62:706–712. [PubMed: 22036995]
107. Chappell MA, McConnell FAK, Golay X, et al. Partial volume correction in arterial spin labeling perfusion MRI: A method to disentangle anatomy from physiology or an analysis step too far? Neuroimage 2021;238:118236. [PubMed: 34091034]
108. Petr J, Mutsaerts HJMM, Hofheinz F, et al. Comparison of two methods for atrophy-correction in perfusion imaging: Partial-volume correction versus gray-matter volume covarying. In: European Society of Magnetic Resonance in Medicine and Biology. 2017.
109. Lee C, Lopez OL, Becker JT, et al. Imaging cerebral blood flow in the cognitively normal aging brain with arterial spin labeling: implications for imaging of neurodegenerative disease. J. Neuroimaging 2009;19:344–352. [PubMed: 19292827]
110. Pettigrew C, Soldan A, Zhu Y, et al. Cognitive reserve and rate of change in Alzheimer's and cerebrovascular disease biomarkers among cognitively normal individuals. Neurobiol. Aging 2019 doi: 10.1016/j.neurobiolaging.2019.12.003.
111. Plassman BL, Williams JW Jr, Burke JR, Holsinger T, Benjamin S. Systematic review: factors associated with risk for and possible prevention of cognitive decline in later life. Ann. Intern. Med 2010;153:182–193. [PubMed: 20547887]
112. Lendahl U, Nilsson P, Betsholtz C. Emerging links between cerebrovascular and neurodegenerative diseases-a special role for pericytes. EMBO Rep. 2019;20:e48070. [PubMed: 31617312]
113. Dolui S, Tisdall D, Vidorreta M, et al. Characterizing a perfusion-based periventricular small vessel region of interest. Neuroimage Clin 2019;23:101897. [PubMed: 31233954]

114. Van Osch MJP, Teeuwisse WM, Van Walderveen MAA, et al. Can arterial spin labeling detect white matter perfusion signal? Magn Reson.Med 2009;62:165–173. [PubMed: 19365865]
115. Skurdal MJ, Bjornerud A, van Osch MJP, Nordhoy W, Lagopoulos J, Groote IR. Voxel-Wise Perfusion Assessment in Cerebral White Matter with PCASL at 3T; Is It Possible and How Long Does It Take? PLoS.One 2015;10:e0135596–. [PubMed: 26267661]
116. Tortora D, Mattei PA, Navarra R, et al. Prematurity and brain perfusion: Arterial spin labeling MRI. Neuroimage Clin 2017;15:401–407. [PubMed: 28603687]
117. Hu HH, Rusin JA, Peng R, et al. Multi-phase 3D arterial spin labeling brain MRI in assessing cerebral blood perfusion and arterial transit times in children at 3T. Clin. Imaging 2019;53:210–220. [PubMed: 30439588]
118. Avants BB, Duda JT, Kilroy E, et al. The pediatric template of brain perfusion. Scientific data 2015;2:150003. [PubMed: 25977810]
119. Carsin-Vu A, Corouge I, Commowick O, et al. Measurement of pediatric regional cerebral blood flow from 6 months to 15 years of age in a clinical population. Eur. J. Radiol 2018;101:38–44. [PubMed: 29571799]
120. Zun Z, Shankaranarayanan A, Zaharchuk G. Pseudocontinuous arterial spin labeling with prospective motion correction (PCASL-PROMO). Magn. Reson. Med 2014;72:1049–1056. [PubMed: 24243585]
121. Václavů L, van der Land V, Heijtel DFR, et al. In Vivo T1 of Blood Measurements in Children with Sickle Cell Disease Improve Cerebral Blood Flow Quantification from Arterial Spin-Labeling MRI. AJNR Am. J. Neuroradiol 2016;37:1727–1732. [PubMed: 27231223]
122. De Vis JB, Hendrikse J, Groenendaal F, et al. Impact of neonate haematocrit variability on the longitudinal relaxation time of blood: Implications for arterial spin labelling MRI. Neuroimage Clin 2014;4:517–525. [PubMed: 24818078]
123. Biagi L, Abbruzzese A, Bianchi MC, Alsop DC, Del Guerra A, Tosetti M. Age dependence of cerebral perfusion assessed by magnetic resonance continuous arterial spin labeling. J. Magn. Reson. Imaging 2007;25:696–702. [PubMed: 17279531]
124. Kandel BM, Wang DJJ, Detre JA, Gee JC, Avants BB. Decomposing cerebral blood flow MRI into functional and structural components: a non-local approach based on prediction. Neuroimage 2015;105:156–170. [PubMed: 25449745]
125. Gousias IS, Edwards AD, Rutherford MA, et al. Magnetic resonance imaging of the newborn brain: manual segmentation of labelled atlases in term-born and preterm infants. Neuroimage 2012;62:1499–1509. [PubMed: 22713673]
126. Shi F, Yap P-T, Wu G, et al. Infant brain atlases from neonates to 1- and 2-year-olds. PLoS One 2011;6:e18746. [PubMed: 21533194]
127. NITRC: UNC Human Brain Atlas: Tool/Resource Info https://www.nitrc.org/projects/unc_brain_atlas/. Accessed May 8, 2021.
128. Ouyang M, Liu P, Jeon T, et al. Heterogeneous increases of regional cerebral blood flow during preterm brain development: Preliminary assessment with pseudo-continuous arterial spin labeled perfusion MRI. Neuroimage 2017;147:233–242. [PubMed: 27988320]
129. Kim HG, Lee JH, Choi JW, Han M, Gho S-M, Moon Y. Multidelay Arterial Spin-Labeling MRI in Neonates and Infants: Cerebral Perfusion Changes during Brain Maturation. AJNR Am. J. Neuroradiol 2018;39:1912–1918. [PubMed: 30213808]
130. Proisy M, Bruneau B, Rozel C, et al. Arterial spin labeling in clinical pediatric imaging. Diagn. Interv. Imaging 2016;97:151–158. [PubMed: 26456912]
131. Morris EA, Juttukonda MR, Lee CA, et al. Elevated brain oxygen extraction fraction in preterm newborns with anemia measured using noninvasive MRI. J. Perinatol 2018;38:1636–1643. [PubMed: 30254332]
132. Makki MI, O'Gorman RL, Buhler P, et al. Total cerebrovascular blood flow and whole brain perfusion in children sedated using propofol with or without ketamine at induction: An investigation with 2D-Cine PC and ASL. J. Magn. Reson. Imaging 2019;50:1433–1440. [PubMed: 30892782]
133. Leeman-Markowski B Review of MRI-Negative Epilepsy. JAMA Neurol. 2016;73:1377–1377.

134. Gajdoš M, Říha P, Kojan M, et al. Epileptogenic zone detection in MRI negative epilepsy using adaptive thresholding of arterial spin labeling data. Sci. Rep 2021;11:10904. [PubMed: 34035336]

135. Pizzini FB, Farace P, Manganotti P, et al. Cerebral perfusion alterations in epileptic patients during peri-ictal and post-ictal phase: PASL vs DSC-MRI. Magn. Reson. Imaging 2013;31:1001–1005. [PubMed: 23623332]

136. Fallatah SM, Pizzini FB, Gomez-Anson B, et al. A visual quality control scale for clinical arterial spin labeling images. Eur Radiol Exp 2018;2:45. [PubMed: 30569375]

137. Boscolo Galazzo I, Mattoli MV, Pizzini FB, et al. Cerebral metabolism and perfusion in MR-negative individuals with refractory focal epilepsy assessed by simultaneous acquisition of (18)F-FDG PET and arterial spin labeling. NeuroImage. Clinical 2016;11:648–657. [PubMed: 27222796]

138. Chen DY-T, Kuo Y-S, Hsu H-L, et al. Loss of labelling efficiency caused by carotid stent in pseudocontinuous arterial spin labelling perfusion study. Clin. Radiol 2016;71:e21–7. [PubMed: 26620708]

139. Barkeij Wolf JJH, Foster-Dingley JC, Moonen JEF, et al. Unilateral fetal-type circle of Willis anatomy causes right-left asymmetry in cerebral blood flow with pseudo-continuous arterial spin labeling: A limitation of arterial spin labeling-based cerebral blood flow measurements? J. Cereb. Blood Flow Metab 2016;36:1570–1578. [PubMed: 26755444]

140. Qu Y, Kong D, Wen H, et al. Perfusion measurement in brain gliomas using velocity-selective arterial spin labeling: comparison with pseudo-continuous arterial spin labeling and dynamic susceptibility contrast MRI. Eur. Radiol 2022;32:2976–2987. [PubMed: 35066634]

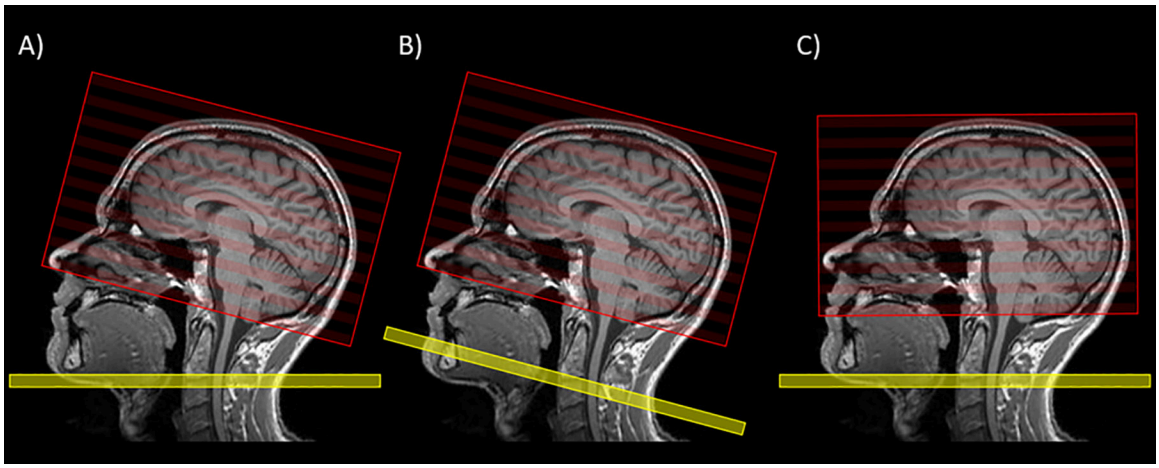

Figure 1:
ASL planning. In A), the labeling plane (yellow) and the image volume (red) can be moved freely and independently. In this ideal case, the labeling plane should be placed perpendicular to the carotid arteries around C2/C3 and the image volume along the AC-PC line in concordance with other used transversal sequences. In B) and C) the labeling plane and the image volume are not individually moveable but follow each other. In B) the orientation of the image volume corresponds to the standard orientation (i.e. the AC-PC line) and can be more easily compared to other conventional MR sequences; however, the radiologist must accept a potential reduction in the labeling efficiency that may vary (for example) between the anterior and posterior circulation. In C) the orientation of the imaging volume deviates from the AC-PC line, but the labeling efficiency should not be compromised. Ideally, option (A) is used and will lead to both optimal labeling efficiency and a familiar imaging slice orientation. When A) is not attainable, the decision between B) and C) rests upon the neuroradiologist and should consider the interpretative objectives of the particular case, though more uniform labeling efficiency is typically desired to avoid regions of artifactual hypoperfusion.

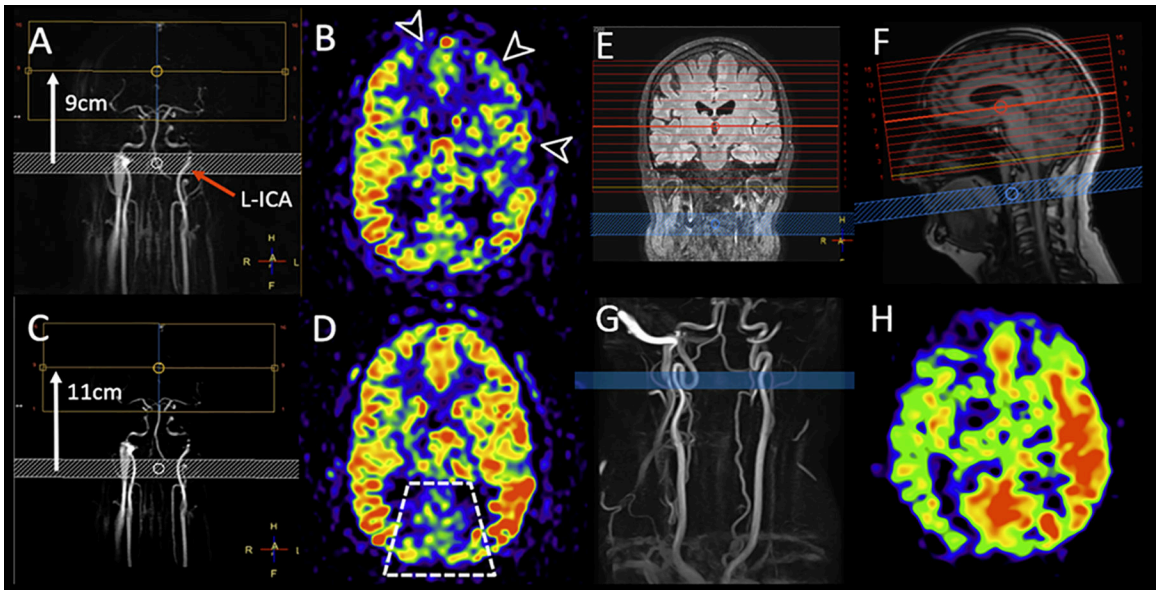

Figure 2:

Two examples of the effect of labeling asymmetry on the CBF images (CBF values are not indicated).

A-D: Two consecutive 3D PCASL scans were acquired in the same MRI exam in a patient at a chronic stage of carbon monoxide intoxication. Both scans were planned on a 2D coronal phase contrast MRA (A and C). B and D show the same imaging slice position. In the first run (top row) the labeling distance was 9cm (white arrow on A). Extensive low signal is seen in the territories of the left middle cerebral artery (MCA) and bilateral anterior cerebral arteries (ACA) (arrow heads on B). On the second run (bottom row) the labeling plane was moved down by 2cm, while the other sequence parameters were unchanged. Note that the left ICA (red arrow) is more obliqued relative to the labeling plane on A, while it is more perpendicular to the labeling plane and symmetrical to the right ICA on C. On the second PCASL scan, most of the previously abnormal areas demonstrate increased perfusion, more symmetric with the remainder of anterior circulation territories. This is a case of labeling asymmetry that was corrected with the repositioning of the labeling plane. Also note that the PCA territories show lower signal on both perfusion maps (trapezoid on D), which is a physiological ASL phenomenon often referred to as pseudo-hypoperfusion. It can be observed with the standard (non-fetal) configuration of the posterior cerebral arteries (PCA), with P1 segments arising from the basilar artery, and it is likely caused by a lower labeling efficiency of the vertebral arteries blood flow compared to the ICAs. (Adapted from Pinter et al. (30).

E-H: Example of asymmetric perfusion without obvious reason. The planning screenshots (E and F) show the labeling plane (blue) and image volume (red). No hemodynamically relevant stenoses are visible on the neck time-of-flight angiography (G). However, upon closer inspection of the planning angiogram, it was noted that the labeling plane was placed in a tortuous loop of the right ICA. The left ICA was labeled in a straight section, perpendicular to the labeling plane. The final CBF weighted images (H) result in a visible perfusion asymmetry, which could lead to a false positive diagnosis when the underlying reason cannot be determined. Such anatomical variants might not be known in patients, and

this example illustrates well the value of providing the planning strategy for interpreting the final ASL images.

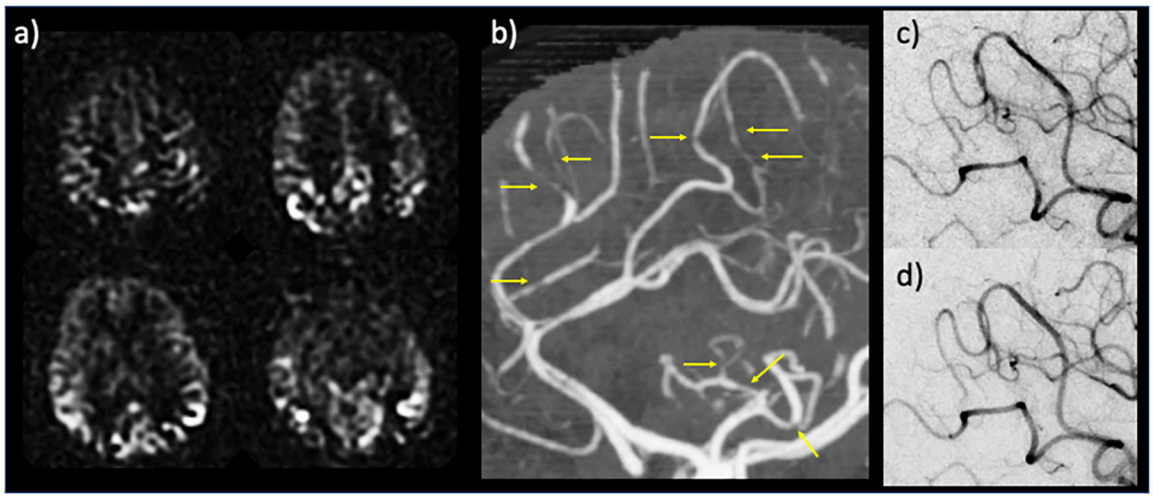

Figure 3.

Example case for the potential diagnostic use of arterial transit artifacts (ATA). 34 year-old postpartum female presenting with severe headache and left-sided weakness. Head CT and CT angiogram initially called negative, without evidence of infarction, large vessel occlusion, or proximal stenosis. Subsequent MRI with ASL demonstrated peripheral curvilinear hyperintensities — i.e., ATA — suspicious for diffuse stenoses versus collaterals (a); retrospective review of CT angiogram revealed multifocal stenosis of distal arterial branches (b, yellow arrows) raising concern for reversible cerebral vasoconstriction syndrome (RCVS). Conventional angiography corroborated the CTA findings of stenosis (c), which reversed after administration of calcium channel blockers (verapamil) (d), thus confirming RCVS diagnosis. In (a) perfusion maps are shown.

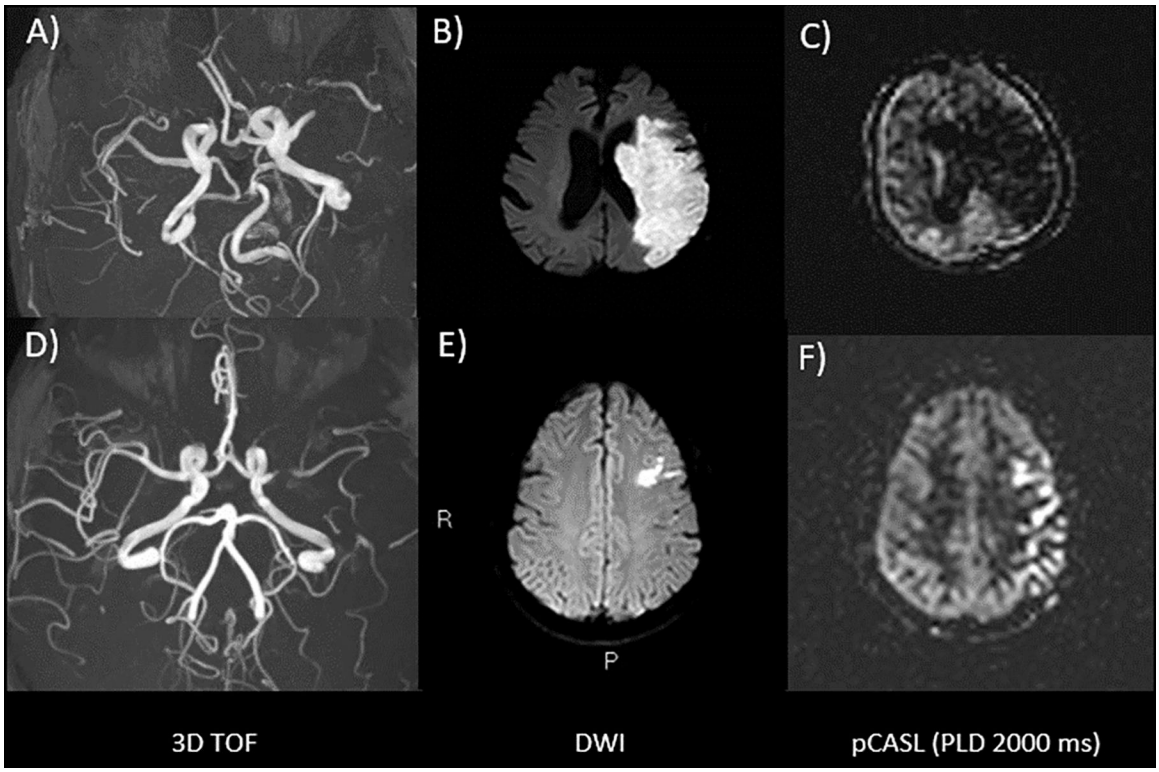

Figure 4:

Two patients with an AIS in the left MCA territory. The first patient in the upper row (A-C) has poor collaterals. The TOF angiogram (A) shows occlusion of the left M1 segment, which has resulted in a large infarct on DWI (B). On the perfusion-weighted ASL image with a PLD of 2000ms (C), there is no visible ATA, indicating a lack of collateral vessels. The second patient (D-F) has robust collaterals. The TOF (D), shows severe narrowing/near occlusion of the left M1 segment and DWI (E) demonstrates a much smaller acute infarct than in the first patient. On the perfusion-weighted ASL images with a PLD of 2000ms (F), there is a serpiginous high signal overlying the left hemisphere. These reflect ATA and presumably correspond to labeled spins in leptomeningeal collateral vessels, which have not reached the brain parenchyma at the 2000ms PLD, yet provide adequate blood supply to prevent a larger infarction (at least at the time of imaging). Images are shown as perfusion values.

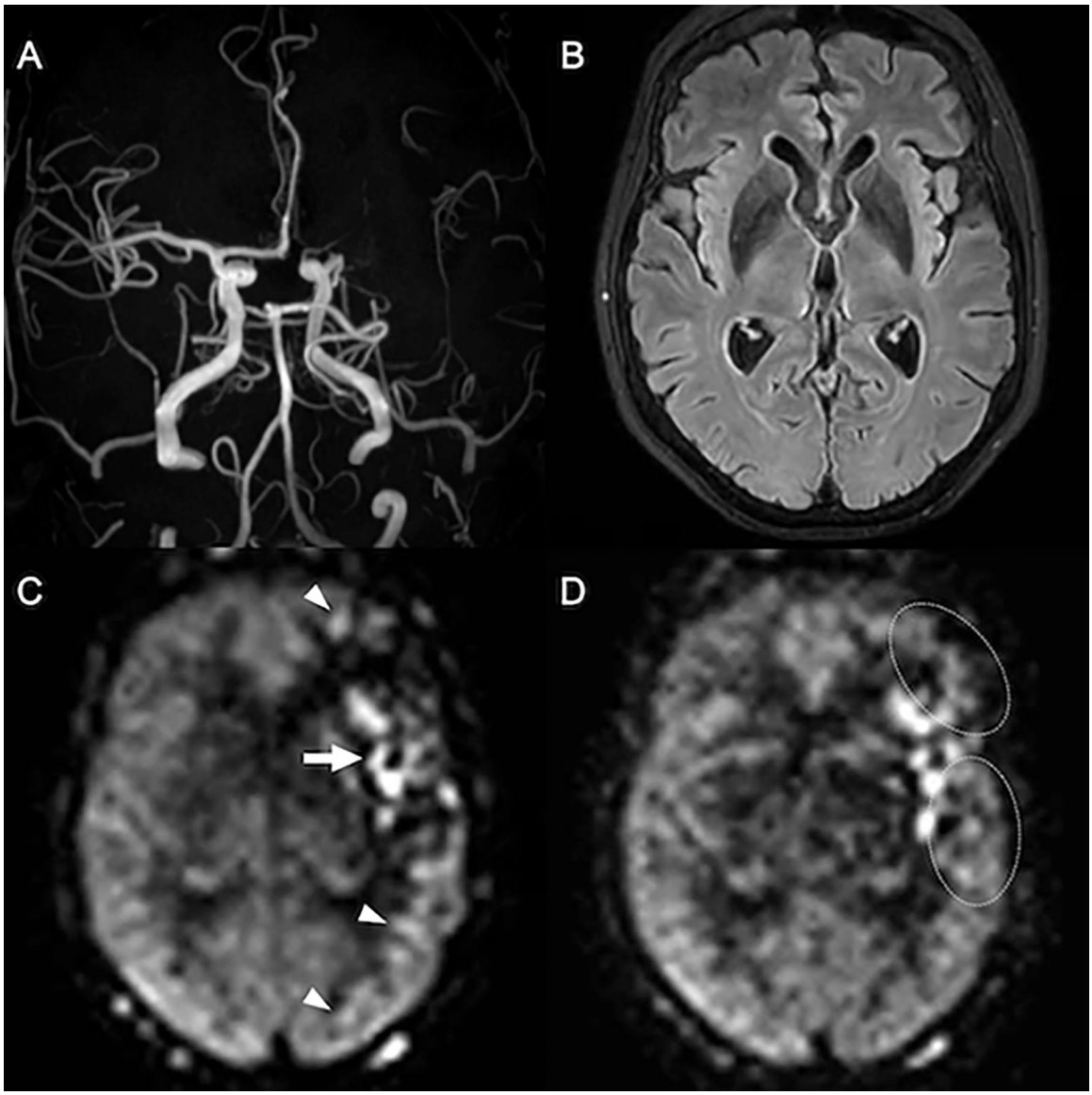

Figure 5:

Delayed arterial flow in chronic ICAD. Normal vasculature and perfusion are seen in the right hemisphere. The left M1 segment has severe chronic stenosis, with diminished signal in distal MCA branches on the Time-of-Flight MRA (A). The corresponding FLAIR image (B) is without findings to suggest a recent infarct, corroborated by a lack of clinical symptoms (note that DWI was not performed). On PCASL with PLD of 1800ms (C) apparent hypoperfusion is seen throughout the left MCA territory, along with arterial transit artifacts in the Sylvian M2 branches and watershed areas (arrow and arrowheads). On a second PCASL with PLD of 2500ms (D) the perfusion signal in the posterior temporal lobe and in the watershed areas normalizes (dotted circles) and the artifacts are markedly reduced, indicating that perfusion is maintained via delayed (collateral) flow. Macrovascular artifacts remain in the Sylvian fissure, consistent with an arrival time >2500ms in these branches, likely persistent ATA. Estimating CBF in the parenchyma fed by these vessels is

possible with PLD >2500ms, although the reduction of signal with T1 relaxation will further decrease SNR. (C) and (D) are perfusion maps.

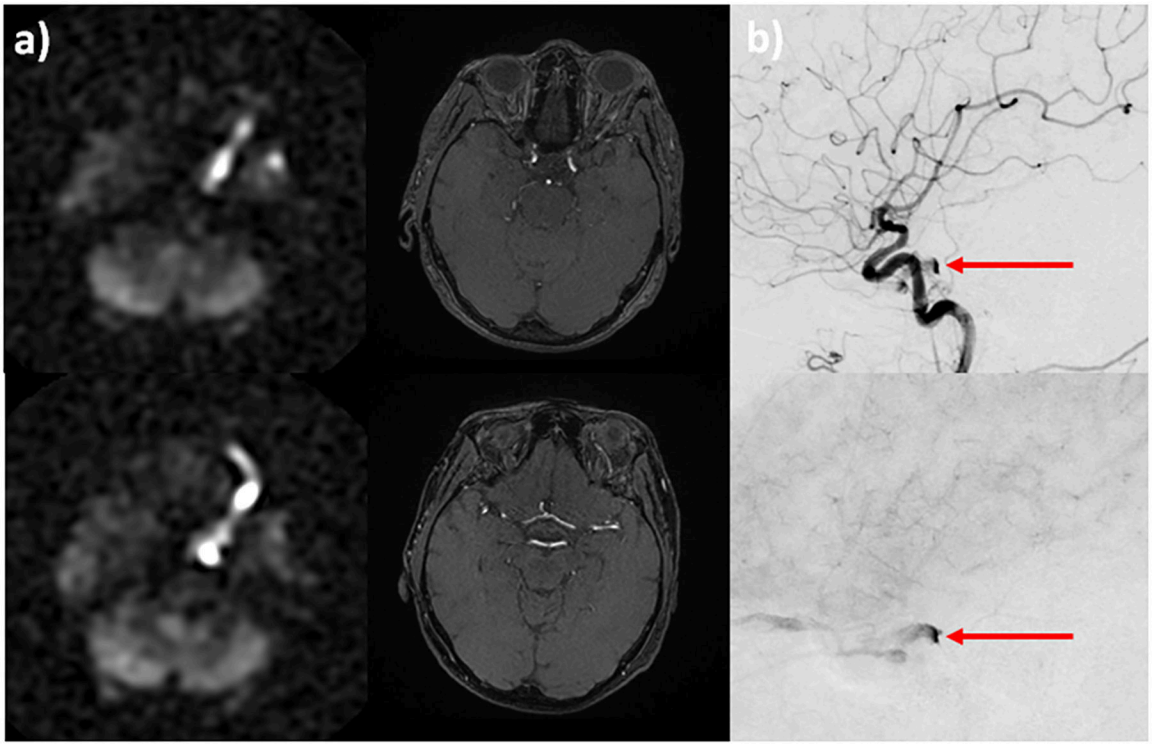

Figure 6:

A 80-year-old woman presents with diplopia, dizziness, and incoordination. Conventional MR imaging was unremarkable. PCASL demonstrates a markedly hyperintense signal within the left cavernous sinus and superior ophthalmic vein, SOV (a, left column). Time-of-flight MRA shows only subtle flow-related enhancement within the left SOV (a, right column). Suspicion of cavernous-carotid fistula was raised based on the ASL perfusion maps. Conventional angiography confirms the diagnosis and shows early venous drainage into the left cavernous sinus and SOV on arterial (b, top) and parenchymal (b, bottom) phase imaging (b, red arrow).

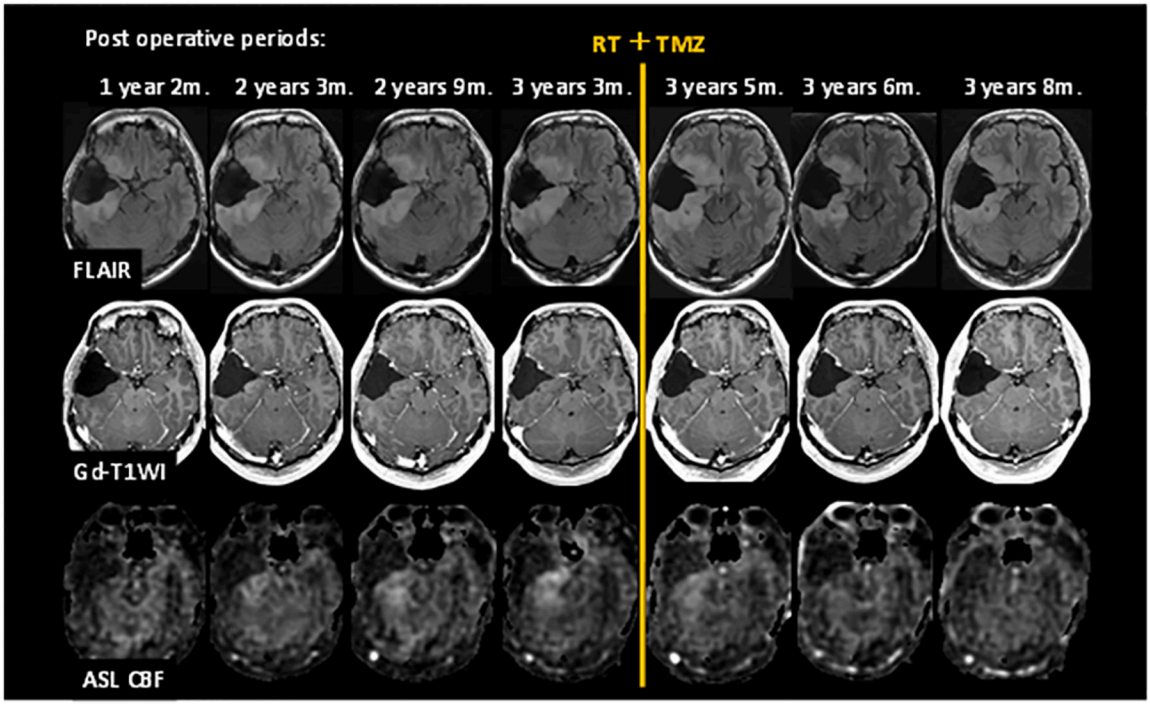

Figure 7:

Exemplary post-operative follow-up MRI examinations using ASL. A patient with grade II glioma underwent brain tumor resection. Images are FLAIR, Post-Gd T1-WI, and ASL CBF from top to bottom rows. CBF images show increasing tumor blood flow before treatment, followed by a decreased tumor blood flow after radiation and temozolomide therapy.

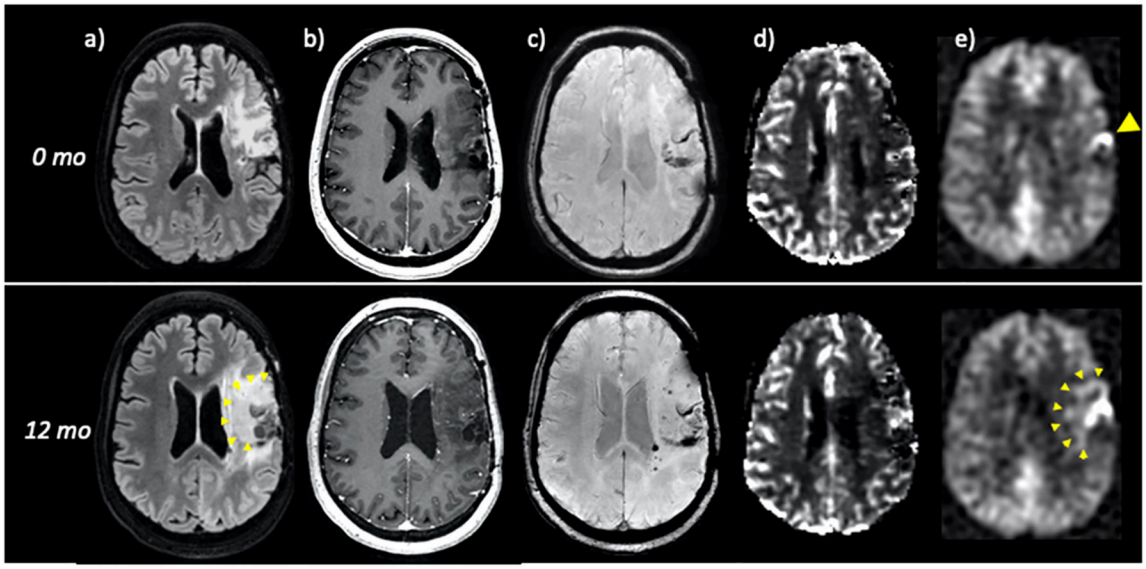

Figure 8:

40-year-old woman with previously resected and radiated left frontoparietal grade III anaplastic astrocytoma. FLAIR (a), post-contrast (b), SWI (c), DSC perfusion (d), and ASL perfusion (e) are shown at time = 0 (top row) and 12 months (bottom row). At time = 0, ASL demonstrates a small focus of hyperperfusion along the resection cavity margins (yellow arrowhead) that raises suspicion for recurrent tumor despite lack of masslike FLAIR abnormality or suspicious enhancement. Importantly, no convincing abnormality is seen on DSC, likely due to susceptibility in the setting of chronic post-surgical blood products (c). At 12 months, there has been marked interval growth, subtly seen on FLAIR and more easily identified by ASL hyperperfusion (yellow arrowheads). DSC again is of poor diagnostic utility and shows only minimal perfusion abnormality.

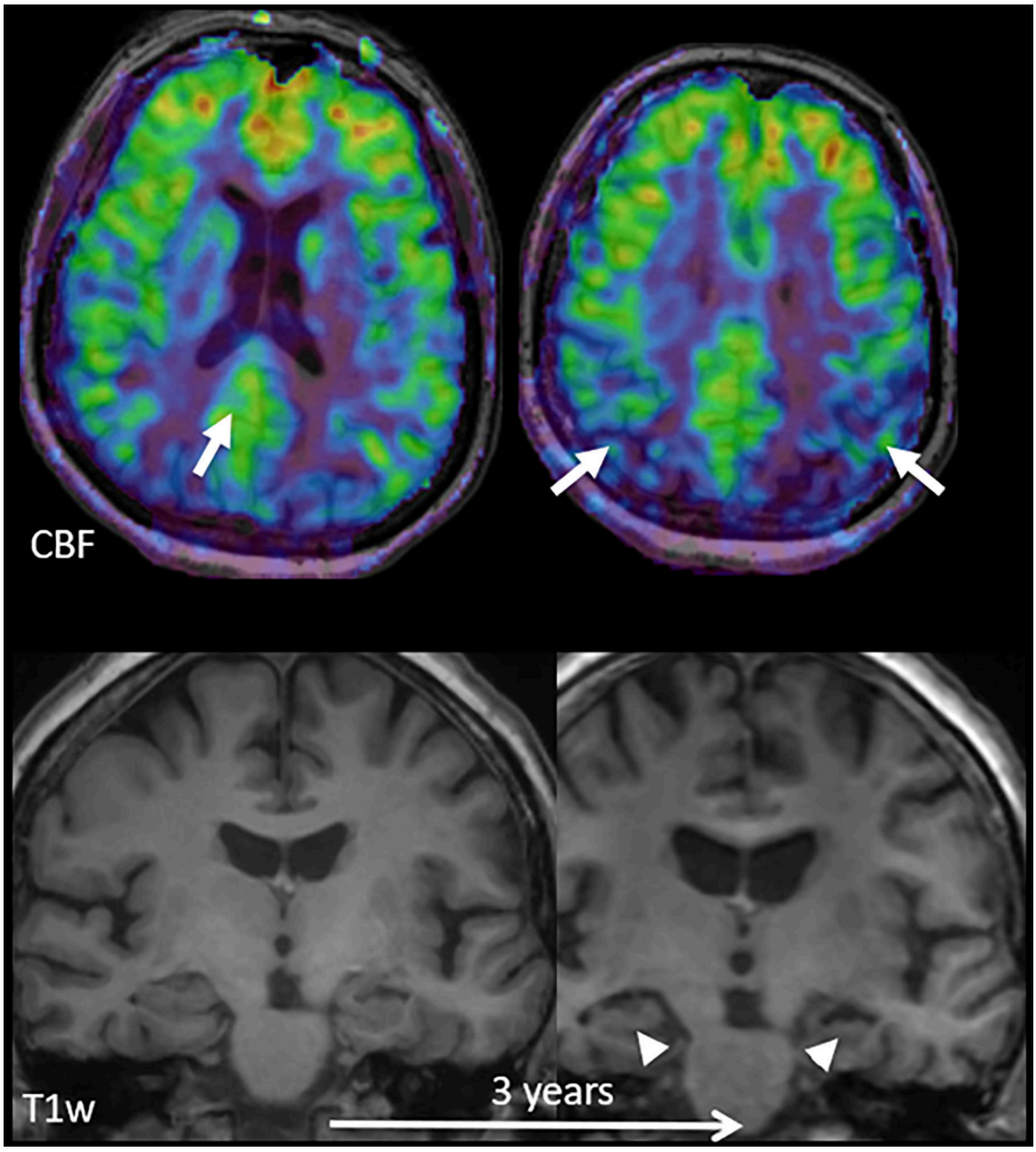

Figure 9:

Early perfusion changes in Alzheimer's disease (AD). Top row: color-coded baseline cerebral blood flow (CBF) maps acquired with ASL overlaid on structural T1w images; bottom row: coronal reconstructions at the level of the hippocampus at baseline and after 3 years. At baseline, hippocampal volume is normal, but hypoperfusion in the posterior cingulate cortex/precuneus (arrow on left) and parietal regions (arrows on right) already suggest AD. Note that the hypoperfusion in the posterior cingulate/precuneus may be missed upon visual inspection, as there is no clear relative perfusion deficit. Perfusion in this area, however, should be much higher than in the rest of the cortex and a quantitative approach confirms the relative hypoperfusion. After 3 years, structural changes consistent with AD,

i.e. hippocampal (arrowheads) and global atrophy, also become visible. Adapted from and courtesy of (2).

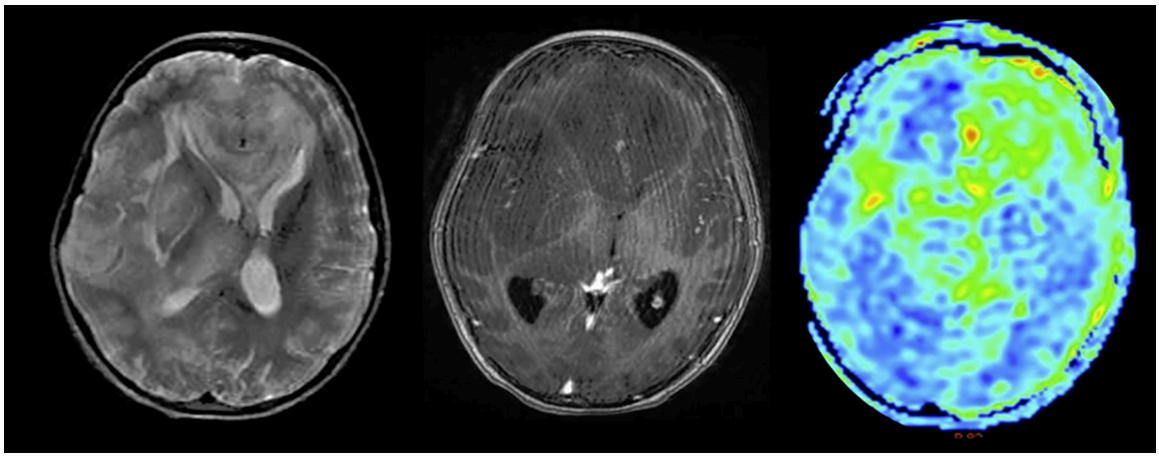

Figure 10:
Case example of a 9-year-old girl. ASL revealing mixed CBF with radiological diagnosis of gliomatosis cerebri (left: T2-weighted; mid: T1 post-contrast; right: CBF map images) with hyperperfused (left frontal) and normo- to hypoperfused (e.g. right frontal) regions.

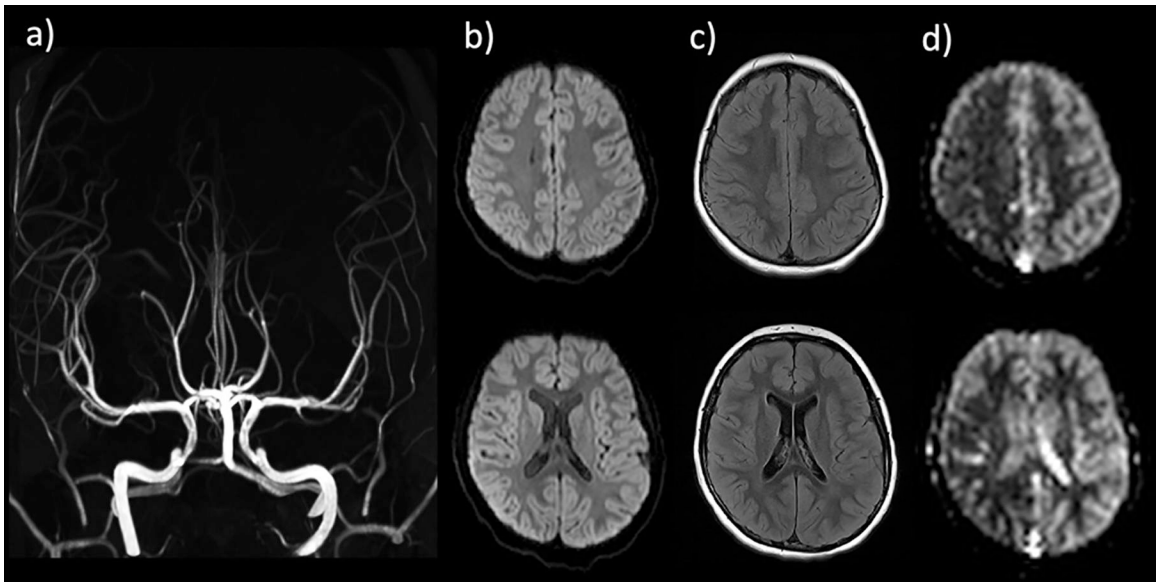

Figure 11.

8-year-old boy presenting with acute-onset left hemiplegia. Stroke protocol MRI without evidence of large vessel occlusion or high grade stenosis on MR angiogram (a), acute infarction on DWI (b), or signal abnormality on FLAIR (c). ASL demonstrates marked CBF reduction throughout the right hemisphere, including the right MCA territory. Based on clinical presentation and ASL findings, diagnosis of complex hemiplegic migraine was made. The patient recovered without intervention.

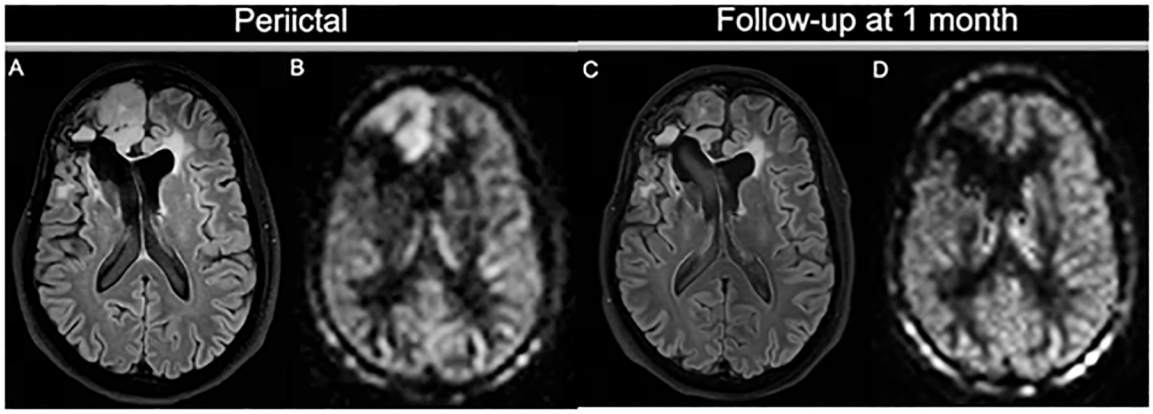

Figure 12:

Seizure activity on ASL. A patient with a history of frontal ganglioneuroma resection 20 years before this presentation had an epileptic seizure, presumably due to encephalomalacia/gliosis. On the peri-ictal MRI, the FLAIR image (A) shows a swollen cortical ribbon in the right medial frontal lobe, with a corresponding increased perfusion signal on 3D ASL (B). Both the FLAIR abnormality and the hyperperfusion are limited to the cortex. Note the contrast between the perfusion signal in the cortex and the subcortical white matter. Lateral to this finding is the stable-appearing surgical cavity with fluid-fluid level and ex vacuo dilation of the right lateral ventricle. At follow-up, the cortical abnormality has almost completely resolved: the cortex is normal size and only minimal FLAIR hyperintensity is visible (C). The ASL scan (D) shows normalized perfusion in the affected region, similar to the left frontal lobe.

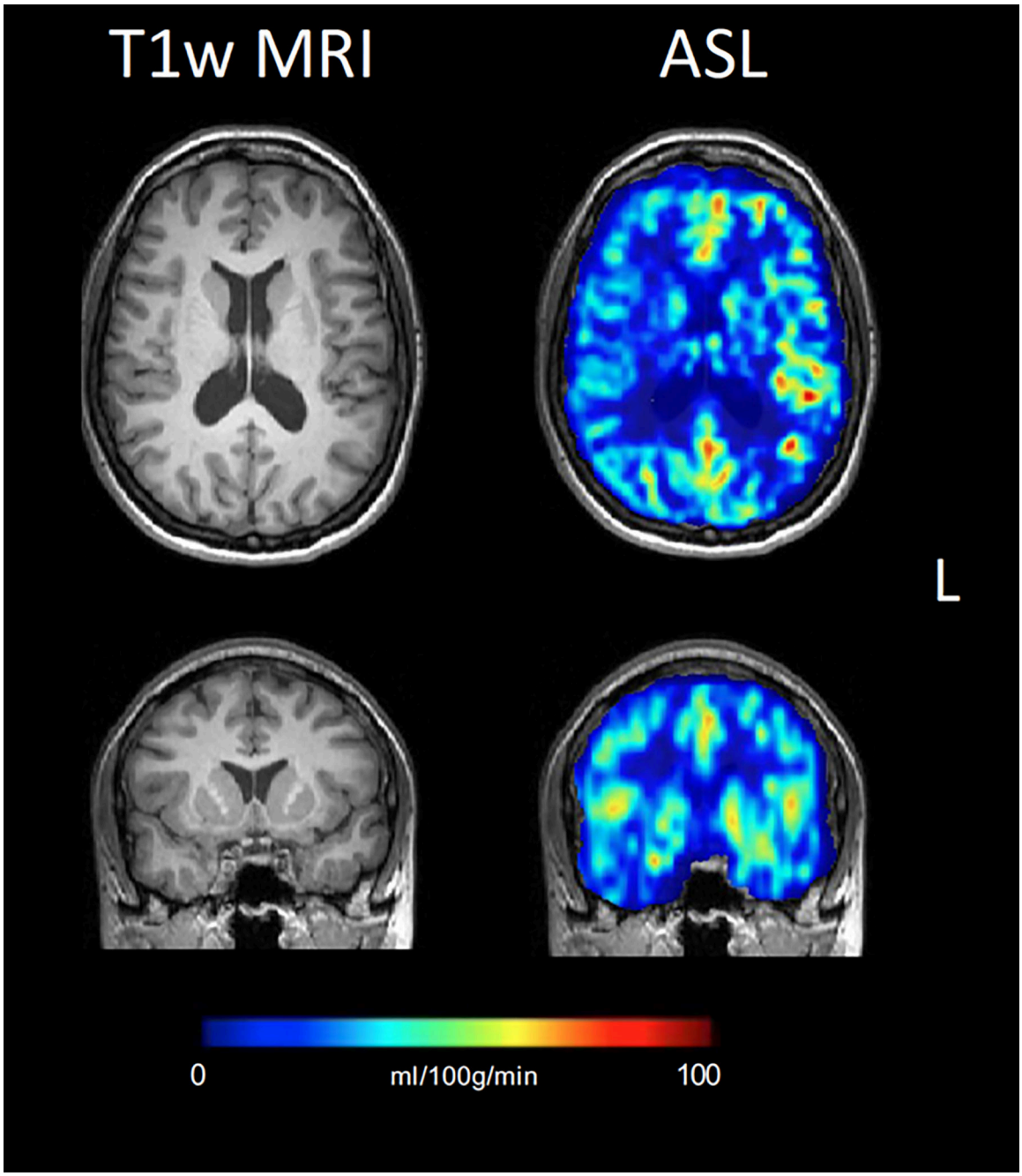

Figure 13:
Interictal ASL CBF map showing right fronto-temporal hypoperfusion in a patient without any morphological-structural alterations identified on structural MRI, but with clinical and EEG localization to the right fronto-temporal lobe and right temporal hypometabolism on interictal PET (not shown).

Table 1:

Recommended physiological and technical information to consider for the report

Technical	
Recommended	**Optional**
Labeling strategy	Vascular crushing
Labeling duration	Background suppression
Postlabeling delay(s) / TI(s)	Number of Control-Label pairs
Physiological/Patient-level	
History of vascular disease	
Medication (especially vasoactive drugs, antihypertensives, and diuretics),	
Caffeine use prior to scanning	
Hepatic/Kidney disease	